Sustainable Energy Technologies and Assessments 45 (2021) 101078

Contents lists available at ScienceDirect

Sustainable Energy Technologies and Assessments

journal homepage: www.elsevier.com/locate/seta

Original article

Strategic examination of the classical catalysis of formic acid decomposition for intermittent hydrogen production, storage and supply: A review

Samuel Eshorame Sanni [a,*], Peter Adeniyi Alaba [b], Emeka Okoro [c], Moses Emetere [d], Babalola Oni [a,e], Oluranti Agboola [a], Amanda Onyinye Ndubuisi [d]

[a] Department of Chemical Engineering, Covenant University, P.M.B 1023, Ota, Nigeria
[b] Department of Chemical Engineering, Faculty of Engineering, University of Malaya, 50603 Kuala Lumpur, Malaysia
[c] Department of Petroleum Engineering, Covenant University, P.M.B 1023, Ota, Nigeria
[d] Department of Physics, Covenant University, P.M.B 1023, Ota, Nigeria
[e] Department of Chemical Engineering, China University of Petroleum, Beijing, China

ARTICLE INFO

Keywords:
Catalyst selectivity
Catalytic dehydrogenation
Copper-active sites
Formate pathway
Hydrogen storage

ABSTRACT

Practically, an ideal catalyst for Formic acid-decomposition is one that best suits the reaction and significantly lowers its activation energy and improves the reaction rate under favourable conditions. Several catalysts for Formic Acid (FA)-decomposition reactions were examined. Based on the volcano curve and the potential of copper to give high hydrogen yields, emphasis was placed on a Cu-catalysed reaction as potential system for sustainable hydrogen production. Some recent advances in hydrogen production from formic acid were discussed and an effective system for FA-decomposition for hydrogen production was proposed. Since helium can be stored in weather balloons and weighs almost the same as hydrogen, a hydrogen buffer made from polyester fabric and coated with polyurethane or a hydrogen cylinder/tube was proposed for storing hydrogen for use as transport-fuel. Also, due to the nature of the mechanisms/pathways describing FA-conversion reactions at the sites or surfaces of the copper-nanocatalysts, it is evident that the Cu(211) coordination site possesses the highest activation energy relative to those of Cu(100) and Cu(111), hence, the reason for the noticeable high or low hydrogen yields. Thus, the potential of Cu giving high hydrogen yields from FA spans from the reactions of FA at the Cu(111) and Cu(100) sites.

Introduction

Hydrogen is an excellent energy carrier, which can be produced from several precursors including natural gas [1] biomethane [2], coal, water [3], formic acid [4], glycerol [5,6], biomass [7] and renewable energy sources. The most abundant sources of hydrogen are hydrocarbons and quite especially, those of the –COOH family [8]. HCOOH has been widely adopted as parent material for hydrogen production because it consists of hydrogen-bonded polymers [9,10]. Without the involvement of catalysts, hydrogen evolution from formic acid occurs slowly, thus giving very low yield. However, in order to improve on hydrogen yield from FA, elements/metals within the transition group of the periodic table are usually employed [11]. According to Bulushev et al. [12], palladium is one of the most prominent catalysts for formic acid disintegration, and due to its slow enhancement of FA-reaction rate, alternative catalysts are being tested for improved hydrogen production [13]. When no catalyst is involved, the decomposition is usually very slow, inefficient and very uneconomical. Due to the time taken for reaction initiation, as well as H_2 generation, several catalysts that possess high time-saving tendencies for FA-breakdown were investigated. According to Sabatier's hypothesis, the most ideal catalyst for a specific reaction must possess the required/minimum binding strength that keeps it in contact with the intermediate products when reaction is in progress [14]. This necessitated a probe into the scientific understanding of the underlying principles of the hypothetical propositions made by Sachtler and Farenfort, where several transition metals were tested as catalysts for effective formic acid decomposition to give hydrogen gas; this then brought to fore, the utmost significance of the "classic volcano

* Corresponding author.
E-mail address: adexz3000@yahoo.com (S.E. Sanni).

https://doi.org/10.1016/j.seta.2021.101078
Received 17 March 2020; Received in revised form 28 December 2020; Accepted 1 February 2021
Available online 2 March 2021

curve" (Fig. 1).

One very important eye-opener of the volcano curve is that it establishes a relationship between the predicted heat of reaction and formation for a specific conversion using several catalysts. Considering the activation temperatures, it is obvious that for 80% conversion of the reactant, the order of preference for the catalysts is Pt, Ir, Ru, Pd, Rh, Cu, Ni, Co, Fe and W. However, due to the costs of Ag and Au as well as the high heat of formations of H_2 with respect to Ni, Co and W, it is advisable to stick to catalysts such as Pt, Ir, Pd, Rh, and Cu owing to their lower heats of formation and activation energy requirements. Also, it is important to note that despite the advantages of each of the catalysts, their limitations were reported to be as a result of the non-anchoring of the catalysts on supports during the reactions. The variation in the data generated, and the normalization of the reaction rate, are due to the bulk catalyst-surface-area, however, low surface areas may result in very slow reactions and errors in reaction rate measurements. This then paved way for the successful introduction of a new parameter tagged the Turn Over Frequency (ToF), which gives the number of molecules of formic acid converted per active-catalyst surface area per second (mass flux) [15]. Also, it was observed that the heats of formation of the intermediates (formates) resulting from the various reactions were calculated using statistical mechanics, which considers the stability of the bulk metal formate, rather than the surface formate formed; this is quite more representative of the supposed reaction intermediate complexes formed by the catalysts. It was also suggested that calculations on bulk metal formates are not appropriate to simulate surface properties of intermediates as they interact with catalysts. A study was conducted on the catalytic decomposition of formic acid using Ag, Au, Pt, Pd, Ru, Ni, Cu, Co, and Fe catalysts. The Temperature-Programmed Decomposition (TPD) spectroscopy and a model-centred approach were used to critically examine the decomposition of FA-surface intermediates (HCOO*) [16]. TPD spectroscopy only measures the superficial properties of formate/intermediates, however, information on the surface kinetics of the preceding step i.e. the adsorption of HCOOH is not feasible with TPD. The surface decomposition of intermediates resulting from formic acid can be seen to exhibit a volcano-type behaviour when the decomposition temperature is plotted on the Sachtler–Fahrenfort chart. This also leads to the conclusion that the slow steady-state scenario of the rate of formic acid decomposition in the presence of Ag and Au catalysts, is largely caused by the adsorption step, which is the rate limiting step [14]. The Sachtler-Fahrenfort volcano curve has also attracted applications with respect to its use alongside the Density Functional Theory (DFT), in areas requiring calculations on formic acid decomposition on multifaceted-metallic surfaces/slabs [17,18]. In recent times, one very significant subject, spurring research interests, is nano-catalysis, owing to the ease with which the single/lone catalysts are sintered to improve their reactivities and stabilities over their bulk counterparts [19]. Of the available groups, nano-transition metals supported on oxides, have been recommended as the most reliable group of catalysts for catalytic reactions [20]; this is as a result of how they are easily synthesized and isolated when the need arises [21]. In addition, the anchor-metals for nanoparticles kinetically serve as the rate controlling steps for catalytic processes [22], whereas, this is not the case for non-supported colloidal

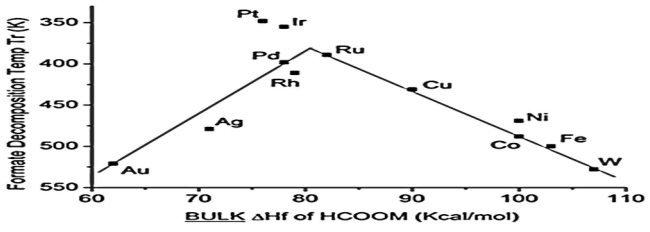

Fig. 1. Classic volcano curve for 80% hydrogen formation from formic acid using unsupported catalysts at varying temperatures. .
Adopted from [6,7]

metal catalysts in semi-homogeneous systems [23]. Although, Sanni et al. [24] synthesized a prominent Cu-tertiary amine catalyst, the chemistry of the synthetic pathway was not studied. This review paper looks into understanding the mechanism and chemistry of the formation step of the formate-intermediate pathway, as one consisting of several elementary steps of the FA-conversion process towards obtaining synthetic hydrogen; the Cu-active sites and coordinates were also examined in relation to hydrogen yield. In addition, efforts were made towards advocating for the recovery of FA from biomass or other chemicals, for further transformation by a reactor system, situated in an automobile, whose engine serves as the source of heat for generating the needed hydrogen as fuel.

Scouting for sustainable hydrogen

In this section, methods of synthesizing H_2 from other sources besides FA, are also discussed. Based on all the works consulted, it is clearly evident that simply considering hydrogen carriers as a sustainable measure for hydrogen production, may not possibly chat the way forward for the existence and commercialization of an economical way of producing hydrogen for use as automobile fuel in IC engines.

Availability status of formic acid from natural sources

In nature, FA is found in the venom of most ants and stingless bees of the genus Oxytrigona. However, the implied venom is a mixture of toxins and irritants (secrotonin, acetylcholine and histamine), of which FA is predominant. John Ray, an English naturalist, was the first person to have successfully isolated FA from the distilled bodies of ants, this was done in 1671 [25]. Wood ants of the genus Formica family can spray FA as a means of attack on their preys, or in defence of their abode/nests against intruders; for instance, the puss moth caterpillar and the carpenter ant often spray FA against their threatening-predators. FA is also present in the trichomes of stinging nettles and there are also speculations of its occurrence in the atmosphere which is traceable to forest emissions. The human body also makes small but harmless/dilute quantities of FA from ingested, inhaled or synthetic methanol. Liquid-FA freezes at 8.3 °C (43 °F) and boils at 100 °C. The name formic acid was coined from the Latin word "Formica", which is the Latin name for "ant". It exists as a pungent, corrosive and colourless liquid comprising of hydrogen bonded dimers [25].

Since current studies have alarmed FA as a major compound from which H_2 can be produced, an appropriate catalyst system that gives high volumetric yield of hydrogen from the parent compound needs be synthesized, with focus directed to obtaining the activation energy of the reaction system. Some catalytic systems with high ToFs have been identified, however, no estimates of the activation energy requirements of such reactions were provided, hence, it becomes necessary that the energy requirements of such reactions are estimated, with a view to identify several potential catalysts that can give high H_2 yield at very low activation potentials. These will provide the necessary information required for efficient designs of suitable fuel housing units in cars for hydrogen storage and thus, inform the type of modifications required in existing IC-engines for their compatibilities with hydrogen gas. Also, it should be noted that reactions beyond 90 °C are not encouraged since a car begins to show signs of over-heating beyond 90 °C. The authors of this paper have also incorporated some of the findings made by Sanni et al. [24] for a formic acid decomposition process where nano-catalysts (copper nanoparticles) supported on triethanolamine were used to speed up the process.

The continuous advocacy for the use of hydrogen as source of power in fuel cells and automobile engines, will not only encourage energy diversification but also reduce the overdependence on fossils as energy sources. Hydrogen undergoes combustion in air to give less emissions relative to fossil fuels. It also combines with air to release its stored H-H bond thereby producing H_2O. It can be stored in pressurized cylinders in

gaseous or liquid forms. Since it barely releases any greenhouse gases during combustion, it is a potential gas for the future if only the prospective CO_2 emissions from the synthetic reactions are carefully minimized. Although, hydrogen can be obtained from several precursors, it barely exists in its free state, hence, it is not a primary source of energy. Also, reports have it that the chemical industries that synthesize NH_3, CH_3OH and refined petroleum, consume about 66% of their yearly H_2-output which is estimated at 35 million metric tonnes. Hydrogen in fuel cells, helps to convert the inherent H-H bond/chemical energy to electrical energy by a process that deviates from that of the Carnot cycle, hence, the energy efficiency of the fuel cell is 2–3 times that of a combustion engine. Polymer-Electronic-Membrane Fuel Cells (PEMFCs) have the capacity to convert the inherent chemical energy in hydrogen, to electrical energy with water released as the only by-product. This serves as a clear justification of the huge potential of hydrogen as an alternative fuel, because, it lowers the energy-burden/over reliance on fossils and generates less-toxic emissions [8]. Therefore, there is no doubt about the perceived role of hydrogen in the near future with consideration for its medium-to-long term effects when used as fuel. With the incorporation of fuel cells in the technology of mobile and stationary systems, large-scale production of H_2 gas will help alleviate the overdependence on crude oil whilst reducing environmental pollution. Formic acid can serve as a sustainable hydrogen source because, it can be sourced from biomass. Thus, cultivating plantations on which these biomasses can be grown is of utmost importance and must be given serious attention. According to Fierro et al. [26], other methods for producing H_2 include:

Steam reforming of Alkanes/Alkanols

H_2 can be recovered from natural gas (NG), naphtha, fuel oil, coal and higher hydrocarbons. However, the high H:C ratio in methane relative to other sources, makes it the most sought-for precursor for H_2-production. The process by which methane is processed to give H_2 is known as Methanol-Steam Reforming; this method is applied industrially owing to the fact that the technology involved is quite affordable and economical [27]. The stoichiometric equation for the reaction is as given below:

$$CH_4 + H_2O \rightarrow CO + 3H_2 \quad (1)$$

Here, NG reacts with steam in the presence of Ni-catalyst in a primary reforming unit at a temperature and pressure range of 1200 K and 20–30 atm respectively. A preliminary pre-treatment stage is necessary owing to the fact that there is need to eliminate the inherent sulphur/mercaptans in the gas. Clean CH_4 is then supplied as feed gas to a reactor containing the Ni-catalyst. Although the exit gas from the reactor is high in H_2 but low in CO, it reacts with water vapour/steam before being converted in a second or third reactor to generate more hydrogen gas. The final product comprises mainly of hydrogen with trace amounts of CO_2 (1% v/v) and excess/unreacted CH_4. Modern H_2-producing plants are designed to incorporate compression, absorption and desorption units in order to improve on the purity of the generated hydrogen gas to as high as 99.99 %v/v. Also, considering the fact that NG contains small amounts of C_2H_6, C_3H_8 and C_4H_{10}, which disintegrate to give carbon residues, a pre-reforming stage becomes very necessary to aid their conversion into CO/H_2. This can be integrated in the upstream reforming unit, thus making it possible to adapt the entire process scheme to a variety of feed stocks. Pre-reforming has a way of influencing the composition of the feed gas in the steam-reforming unit. However, longer chain hydrocarbons can be totally eliminated while fractional/partial methane conversion begins to take place. This is targeted at reducing the tendencies of these long chain carbons giving rise to carbon residues during the reforming process, and thus, preserves the service-life of the catalyst employed in the reforming process. The steam used in the reforming process may be replaced with CO_2, O_2 or their mixture. Advanced reforming units of this sort, are similar to classic steam reforming processes. In particular, this route is employed if it is desired to use the C/H_2 mixture to synthesize hydrocarbons or CH_3OH rather than H_2. Also, instead of CH_4, CH_3OH can be used as raw material for this process, such that, the alkanol is first reacted with steam in the presence of a catalyst to give H_2. Given that the reaction is endothermic, the energy required for the reaction is obtained from the heat of combustion of the tail-gas and a light portion of the methanol-feed. The H_2-stream is then scrubbed in an absorption/desorption unit i.e. a CH_4-reformer. The advantage of this process is that it does not allow for the formation of intermediates/oxygenated constituents. However, for economic reasons, the method is only applied when the methanol to be used is in excess, since part of it is used as fuel for the system. The LPG-content, quantity of distillates recovered and the good distribution network, make these fractions ideal candidates for H_2 production. In lieu of the aforementioned cases, the development of these processes have only gained little attention owing to issues related to catalyst-poisoning by carbon deposits, partial oxidation of the inherent hydrocarbons in the methanol-feed, rise in temperature of the HC-air mixture, expulsion of sulphur in the form of H_2S at the reactor outlet, and steam injection which precedes the water–gas-shift reaction. Considering polymer membrane fuel cells, the CO released from this process must be less than 10 ppm which is achieved by passing the mixture over catalysts that are able to convert the CO to CO_2 at room temperature. The release of poisonous mercaptans and coke deposits, on the surface of the catalyst for this system, is yet to be curtailed, however, in lieu of the impact of this technology on the environment, car manufacturers still deem it a suitable/considerable option to use H_2 as power source for fuel cells. Do et al. [28] succeeded in producing hydrogen from propane via hydrothermal/steam reforming, which was aided by a nickel-based catalyst supported on $AlSi_xO_y$, where they established the effect of acidity on the performance of the catalyst at high temperatures (i.e. 200–600 °C); they adopted a steam to propane ratio of 1:6, which makes the process somewhat highly energy intensive and expensive in terms of overhead cost of the entire process per kg hydrogen produced.

Electrolysis of water

This method is employed for small scale production of H_2. The reaction prevails in an alkaline medium at a controlled pH which helps to boost electrical conductivity. The set-up comprises of terminals (electrodes; cathode and anode) where anions/cations migrate to as soon as electrical pulses are supplied in terms of direct current to the cell. The cathodic hydrogen is impure as it contains certain amounts of O_2 and moisture. The moisture is dried over a suitable adsorbent while the O_2 is eliminated in a deoxo-converter. Oxygen is also produced at the anode, although, its volume is half that produced at the cathode. The electrolytic reactor takes the form of a rectangular tank with parallel electrodes and the heat released is removed by counter current flow of water recirculating around the cells. The disadvantage of this process is the relative cost of H_2 which is worth 4.9–5.6 kWh/m^3, thus making it at least twice as expensive as the H_2 from NG reforming. Since conventional electrolysis produces high-cost hydrogen, other alternative processes being exploited include steam-phase electrolysis where the reversible potential of the cell is lowered as the temperature of the cell increases; since the cost of energy/electrical power required to produce 1 mol of H_2 from water is proportional to the EMF of the cell, it then implies that, the total cost can be reduced by lowering the temperature of the system. Also, since the reaction is endothermic, the system can be maintained at constant temperature which makes cooling easier. Hence, the electrical energy is electrochemically converted to H_2 without necessarily needing to go through an intermediate phase or the energy transition stages of the cycle. Thus, at 1,500 K, the amount of heat spent in the thermo-chemical decomposition of H_2O is 50% of the total energy input of the conventional process. Another electrochemical process or alternative route for H_2-production is one which employs or takes advantage of electro-catalysts at lower voltages, thus reducing the overall cost of H_2 produced. According to the comparative life cycle

analysis of two hydrogen production routes (i.e. the membrane water electrolysis and methane steam reforming) conducted by Bareiß et al. [29], the adoption of membrane water electrolysis depends on renewable energy as the source of electrical energy for the system. Although this system limits CO_2 emissions by 75%, the process is somewhat expensive if it must be commercialized on a large scale; also, the issue of membrane fouling and stability are of paramount concern.

Hydrogen from Thermo-chemical conversion of biomass

Hydrogen in biomass can be obtained via thermo-chemical processes (combustion, liquefaction, pyrolysis and gasification). Firstly, the biomass is partly oxidized above 1000 K in order to obtain a gaseous fraction as well as carbon residue, which is subsequently converted to H_2, CO, CO_2 and CH_4. Aerobic biomass gasification generates a H_2-rich stream which is reformed at the water vapour gasifier-exit to release additional hydrogen. A major shortcoming in hydrogen recovery from biomass gasification is the formation of tar or ash which increases the tendencies for catalyst poisoning [27]. The resulting heavy residues/components undergo polymerization which give rise to complexes that do not favour the H_2-production process. Tar formation can be controlled by retrofitting the gasifier and integrating self-repairing catalysts as well as, adjusting the operating conditions and process variables; the proposed catalysts will help to lower tar formation, improve the quality of H_2 produced and enhance the conversion of the intermediate product/gas. On the other hand, ash formation can cause a build-up of solids on the catalyst-surface, which subsequently plugs and deactivates the catalyst, although, this can be controlled by ash extraction and fractionation during the operation in order to reduce the accumulation of these constituents in the reactor or product-channels during the process.

Hydrogen from Microbes: Fermentation and photosynthesis (Bio-photolysis)

This method takes advantage of bio-photosynthetic/non-photosynthetic microorganisms (*Scenedesmus*/green algae, *Cyanobacteria- Spirulina* species etc.), which are able to breakdown water molecules into its constituents (H_2 and O_2) in the presence of visible light or under anaerobic conditions in the absence of light. Reports have it that, the *Scenedesmus* species is not only able to stimulate H_2 production by irradiation of light, but can also produce H_2 via fermentation under anaerobic conditions with starch as starting material. However, the produced H_2 obtained by fermentation is more stable relative to that from photosynthesis owing to the absence of oxygen. Despite the low investment cost involved in this process, the challenge with producing hydrogen by this method still remains "non-commercialization", caused by the low energy efficiency of converting solar power to chemical energy by the aforementioned biological systems/microbes. Evidence has it that, photoheterotrophic microorganisms have a 7% maximum conversion efficiency of solar power to chemical energy. Furthermore, biological reactors have also been exploited for use in producing hydrogen. These reactors require less energy, ambient temperature and pressure, with the requisite advantage of bypassing CO_2 production, which may result in terrible consequences for the electrodes of a fuel cell. Two routes are involved in the hydrogen production process, and these include fermentation and photosynthesis. The photosynthetic step is either aided or non-aided by oxygen. Other aerobic photosynthetic microbes include *Chlamydomonas* and *Rheinhardtii,* while an example of the anaerobic photosynthetic ones are the *Rhodobacter spaeroides*. Microbes such as *Escherichia coli*, *Clostridium* and *Enterobacter species*, that undergo fermentation to produce hydrogen, have been studied [30–34]. According to literature, the hydrogen production per cell obtained in a fermentation process is higher than that obtained from photosynthesis. Bio-hydrogen production rates of 151.2 mg $L^{-1}h^{-1}$ and 605 mg $L^{-1}h^{-1}$ by *Enterobacter cloacae IIT-BT08* and a consortium of mesophilic bacteria, which have an equivalent volumetric flow rate of 7.4 Lh^{-1} at room temperature, are the highest ever-reported hydrogen production rates till date. However, the major concern still remains that such hydrogen production rates are not commercially viable [30,35]. In order to abate this problem, two things to consider include improving on their low H_2-yields and volumetric fluxes. According to Woodward et al. [36], 11.6 mol of H_2 can be generated from 1 mol of glucose 6-phosphate extracted from a microbe. The low quantity of H_2 produced was attributed to the growth rate of the anaerobe, its total cell count and low cell density [37]. Yoshida et al. [38] overcame this problem of low hydrogen production by genetic modification/increase in number of microbial cells which served as catalyst for the reaction, and increased the microbial cell density with subsequent conversion of the formate formed as intermediate product from the glucose into the needed hydrogen. Other substrates that have been used besides glucose include Nicotine Adenine Dinucleotide Hydride (NADH) and Nicotine Adenine Dinucleotide Phosphate Hydride (NADPH); both are intermediates formed from their precursors during the breakdown of glucose which need be oxidized prior the commencement of a new cycle of the conversion process. Furthermore, ferrodoxin, cytochrome which enhances electron transfer as well as formate (the end product) formation, have been identified as promoters of microbial hydrogen synthesis. The active catalysts/enzymes in microbes that help in the catalytic dehydrogenation of formate is the Formate Hydrogen Lyase (FHL) complex, which is present in microbes such as *Enterobacter*, *Methanogenes* and photosynthetic bacteria [39–41]. Fig. 2 gives the hydrogen production rate for different FHL strains experimented by Yoshida et al. [38] where the highest volume of hydrogen recorded was for the SR13 strain with a production rate of 300 mmol/gh after 10 h of production time.

Thermal conversion of H_2O/Metal sulphates

This process simply involves the thermal dissociation of water molecules into molecular hydrogen in nuclear reactors/solar furnaces by the application of heat at high temperatures of less or equal to 950 °C. The generated heat in transit, is used to breakdown water into its constituents (H_2 and O_2) [27]. An example of this kind of process is the thermal decomposition of a metal sulphate first at 1100 K to give a metal oxide alongside SO_2 and O_2. In the second stage, oxidation of the metal oxide to sulphate and H_2 is aided by introducing steam and SO_2. Two major advantages of this process are the zero CO_2 emission and an achievable efficiency of about 85% conversion of water to H_2. However, the method has not been implemented on industrial/commercial scale and it is highly energy intensive.

Photochemical reactions

These reactions result in the splitting of water molecules on a

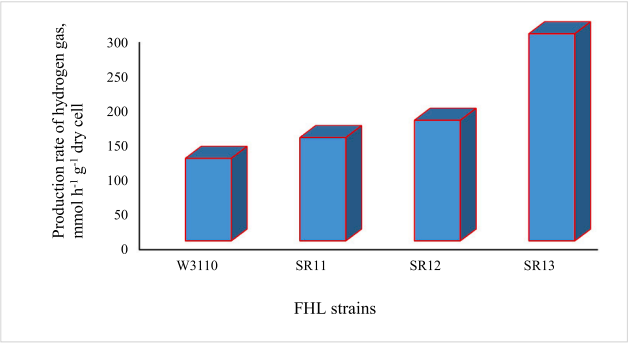

Fig. 2. H_2-Production rate over 10 h culture-resuspension in 50 mL phosphate buffer in the presence of 100 mM sodium formate at an OD610 of 1.0. Adopted from ref. [38]

semiconductor using sunlight. The efficiency of this method is highly dependent on the photo-physical properties of the semiconductor. The limitation of this method is that a thorough understanding of its commercial application requires that the H_2 produced in the visible spectrum photon is further improved with advanced science and engineering principles in order to be able to achieve stable photocatalysts during the dissociation process [27]. Other unresolved issues include, the unravelling of the mechanism behind the charge transfer between the semiconductor and co-catalyst which will help in understanding its dependence on the inherent morphological and interfacial electronic factors. However, these points pose excellent opportunities for improving the photocatalyst-options available for photo-chemically dissociating water. Also, efforts can be directed towards controlling the structures of the catalysts employed at the nanometric scale, which will in turn foster adequate photocatalyst morphology-modulation and reactivity.

Ethanol/sugar reforming

Ethanol and glucose are renewable precursors for H_2. The reforming process involves the use of high-pressure steam in the presence of catalysts. Glucose and ethanol are neutral in terms of CO_2-emmision. One major shortcoming of the process is that other undesirable/by-products such as CO, CH_4 and acetaldehyde are formed as a result of side reactions which also culminate in low H_2-selectivity by the catalyst with subsequent reduction in the volume of H_2 produced [27]. The low amount of H_2 recovered from the process can also be attributed to catalyst deactivation which may be caused by the accumulation of carbon deposits on the catalyst surface; this therefore makes it a herculean task in commercializing the referred reforming process. Furthermore, another major challenge that needs be addressed, is the development of suitable catalysts that will not only operate at lower temperatures but, also help to minimize catalyst-deactivation.

*Thermo-**catalytic dehydrogenation of formic acid***

Thermo-catalytic dehydrogenation reactions of FA involve the decomposition of formic acid aided by some catalysts. The implied catalysts may be used alone or with some form of supports which help to overcome the required barriers as well as hasten the reactions along favourable pathways at the most selectively active catalyst sites. These reactions prevail under unique steps to bring about the formation of hydrogen as well as CO_2. Efforts need also be put in place for the capture of CO_2 since an equivalent amount in mole of CO_2 as obtained for hydrogen, is released during the process. By the experimental procedure discussed in Sanni et al. [24], where a Cu-tertiary amine system was adopted for the first time in producing hydrogen from formic acid, it is evident that, the process guarantees less release of CO_2 by the method of collection (i.e. downward displacement of water) due to CO_2 solubility in water. Furthermore, the hydrogen produced can be passed over limewater ($Ca(OH)_2$) in order to completely strip the gas of CO_2 and other trace gases, this will aim at ensuring the availability of pure hydrogen for storage and fuelling of automobiles. Hence, at a later section, much of the discussions will focus on some of the best published catalysts for high hydrogen production as well as, the use of copper and its special attributes that ensures its reliable use over several cycles (the referred Cu-tertiary amine system has a reusability of 20 cycles in 120 h) [24].

In line with the proposal given in the above paragraph, FA holds a lot of prospects as starting material for sustainable hydrogen production. According to Alotaibi [42], formic acid can be sourced from the earth's abundant biomass, can be handled in its aqueous state, has high-energy density, is nontoxic, and highly stable at room temperature. Based on excerpts from ref. [43] where sensitive parameters were used to describe the intensity of the chemical properties of some hydrogen carriers, it can be seen that HCOOH has the highest flash point amongst all other carriers with the exception of ammonia (Table 1), but owing to the toxic nature of ammonia, FA still gains more preference in terms of being a source material for hydrogen production.

Furthermore, of all the available alternative sources of hydrogen, formic acid has proven to be one of the most benign routes for obtaining synthetic hydrogen. HCOOH as a formate precursor, can be obtained from glycerol, methanol, water and biomass [44,45]. In lieu of the underscored alternatives, formic acid is a very efficient precursor for H_2 production owing to its inherent carrier-property, its relative abundance, good activity with catalysts, high yield and sustainability.

Hydrogen from formic acid

Based on the work of Bulushev et al. [46], hydrogen was produced from FA using Pt/C (1 and 10 wt%), Au/C (0.8 wt%) and TiO_2/C of 1 wt %. The highest selectivity of the catalyst was recorded for the Pt/C catalyst combination at 390 °C, thus producing about 0.04 mol H_2 per minute per gram of the catalyst. In addition, the estimated catalyst selectivity did not simulate conversion but was only a measure of high catalytic activity. Also, particles of lower molecular weights performed better than particles of higher molecular weights owing to their increased surface area to volume ratios. According to them, catalyst-selectivity was found to be weakly dependent on the reaction temperature, conversion and time, although, that is never the case for the actual conversion of FA because, it is temperature dependent. Again, the reaction is highly energy intensive as the best results were achieved at about 663 K, whereas, other catalysts can give better results at mild conditions/lower temperatures. The study by Xue-li et al. [47] involves the synthesis of several ionic liquids including 1-(2-Diisopropylaminoethyl)-3-methylimidazolium chloride (i-Pr2NEMImCl) as catalysts by an approach that bothers on the hermetical storage of an already low-pressure-distilled 1-Methylimidazole of 99% purity. The ionic liquid used as catalyst was produced via several complex steps that are quite time consuming, which in turn make the catalysts, as well as the overall process somewhat expensive. Amongst the tested ionic liquids, i-Pr2NEMImCl-HCOONa gave the highest activity with a ToF > 600 mol/mol/h. The highest volume of hydrogen produced was 1057 mL in 2 h, thus giving an hourly production rate of 528.5 mL for 5 moles of catalyst used. Although the reaction temperature was 60 °C, the process routes for the ionic liquid-catalyst syntheses involved several chemicals that made the entire process somewhat complex. Secondly, the catalysts assumed the form of hybrid chemicals/compounds which increase the overhead cost of the entire process. An additive-free formic acid decomposition was carried out at 30–60 °C using Pd/C catalyst. Catalyst selectivity was found to be > 99.9% with a turn over frequency of about 1136 h^{-1} [48]. Despite how wonderful this catalyst performed, no information was given as regards the number of cycles required to produce the highest volume of hydrogen before catalyst poisoning sets in and the threshold tendency for steric hindrance. Also, palladium cannot be easily sourced as it is a precious metal like gold and platinum, hence, it is considered expensive. The authors used a High-Performance Liquid Chromatograph to determine the FA-conversion. Hydrogen production

Table 1
Chemical properties of hydrogen carriers.

Parameter	Formic acid	Methanol	Ethanol	Ammonia
H_2 content (wt. %)	4.4	12.5	13	17.7
Hazard codes	C	F,T	F	T,C,N
Risk statements (R-phase)	R10, R35	R11,R23-25, R39	R11	R10,R23,R34, R50
Boiling point (°C)	101	64.7	78	−33
Explosion limits (Upper-lower vol. %)	18–57	6–36	3.3–19	15–25
Flash point (°C)	48	9.7	14	132

Source: Adopted from [43].

was simulated and optimized by performing periodic plane-wave DFT simulation adopted from a Vienna ab-initio simulation package (VASP). The durability or reusability of the catalyst, dropped from 84% to 72% between the 2nd and 5th cycles in 1.5 h. According to them, the Pd/C catalyst had its catalytic activity retained by about 72% of its initial activity at its fifth time of use. However, despite washing and keeping the catalyst dry for 18 h before each cycle, they allotted that the slightly evidenced decrease in the catalyst activity may have been caused by: the absorption of FA onto the surface of the catalyst, CO-poisoning as well as the nano-Pd agglomeration or drop in Pd loading caused by leaching, as evidenced by the low concentration of Pd in the supernatant solution analysed with Absorption Electron Microscopy. The investigation conducted by Muller et al. [49] is a comparative study of hydrogen synthesis from two process routes during FA decomposition and water electrolysis. Their advocacy as regards FA-decomposition is in the direction of controlling the reactions to give a formate rather than the carboxyl as intermediate product; this abates the tendency of producing formic acid from CO_2 and H_2O which gives lower conversions. Based on their findings, the formate route is more cost effective relative to the carboxyl route. Also, according to them, the splitting of water in the hydration step is way more expensive than going through the formate-formation step. The enthalpy of decomposition has a high significant influence on the total energy demand of the reaction system. They also asserted that the over dependence on FA-concentration by the bicarbonate route is due to the large heat capacity of the accompanying water at the dehydration stage; thus, the amount of heat required by the process can be quantified in terms of the rate of evaporation of water at the dehydration stage. However, they concluded that with the help of a catalyst, the heat requirement reduces to about 6 kJth per mole FA, for step temperature increases of 20–80 °C.

Reaction Pathways, mechanisms and structural sensitivity of FA on Cu catalysts when used with, or without any support

FA (HCOOH) has spurred research interests as one of the major by-products in biomass conversion; it is a carrier of hydrogen gas, and a source of fuel for fuel cells. In spite of the few experimental studies on HCOOH-decomposition as aided by Cu-catalysts, the mechanism of the reaction and its structural sensitivity are still far from being well-understood. In the study by Li [50], self-consistent, three model copper coordination sites i.e. Cu(1 1 1), Cu(1 0 0) and Cu(2 1 1), were examined along two basic routes, they include the formate (HCOO)- and carboxyl (COOH)-mediated pathways. Based on their findings, the path defined by their energy studies, suggest that the formate mediated route holds more prospects than the carboxyl-mediated route at the coordination sites. According to them, FA-decomposition occurs in two steps, which is immediately preceded by hydrogen desorption. The formate group as compared to the carboxyl group is the rate determining step, owing to its higher transition state and activation energy which are characterized by the three catalytic steps along the HCOO-route. The decomposition was found to be Cu-structure sensitive, and based on the analysis, all three Cu-catalyst facets exhibited different binding strengths for the intermediate "HCOO" while having close activation energies during dehydrogenation. The coordination sites of Cu(1 0 0) and Cu(2 1 1) were seen to bind the formate (HCOO) much more than the Cu(1 1 1) coordination site due to their lower potential energy surfaces relative to Cu(1 1 1). Under the reaction conditions, there may be a substantial surface coverage of the HCOO-intermediate by H_2, which may convert the intermediate to its stable form/corresponding acid and store the acid under-coordinated corners or defective sites. HCOOH acid decomposition is said to be most likely prevalent at the terrace sites of Cu nanoparticles. Studies have also shown that vapour-phase decomposition of FA is a widely known test for examining the catalytic features of metals [51–54] and their oxides [55–57] including alloys. FA is one of the most common organic-molecules which can be split on metal surfaces via a dehydrogenation or dehydration scheme, both leading to the formation of CO_2 and H_2 as well as, H_2O and CO respectively; the two schemes are interlinked by a water gas shift (WGS) reaction. CO is a known catalyst poisoner for Cu, Pt, Pd and several other catalysts. Furthermore, Cu can selectively decompose FA via the dehydrogenation step to give CO_2 and H_2 without CO being produced [58], however, this requires impeding the WGS-reaction step. Other researchers have recorded similar results for temperature programmed reactions of FA on Cu with single crystal surfaces [59–62], while spectroscopic studies have helped to identify the reason behind this occurrence. However, some researchers have recounted that it is caused by the existence of a stable formate group/intermediate which results from the adsorption of H_2 on the surface of Cu [62]. Iglesia and Boudart [58] based their investigation on the formate reaction-pathway, where they obtained an activation energy of 94.5–100 kJ/mol for FA-decomposition using Cu catalysts on different supports; same results were obtained for preferentially oriented (PO)- and polycrystalline (PC)-Cu catalysts [63–65]. Their investigation led to the conclusion that there was no direct correlation between the observed turnover rates (TORs)/Turn over Frequencies (TOFs) of hydrogen and the particle-size of copper as well as the catalyst support. Furthermore, they asserted that FA decomposition on Cu is not structure-sensitive, however, Nakano et al. [66] gave a contrary opinion stating that the FA-decomposition was structure sensitive with varying activation energies for the dehydrogenation of the formate-intermediate with respect to the Cu(1 1 1) and Cu(1 1 0) coordination sites. They added that formate formation from the CO_2-evolution step was structure insensitive at the two Cu coordination sites. The strong dependence of the energy of adsorption of FA onto the surface of Cu was also confirmed by Hu and Boyd [67], and they opined that the energy of FA adsorption onto Cu sites is in the following decreasing order of magnitude i.e. Cu (1 1 0) > Cu(1 0 0) > Cu(1 1 1). Some researchers have also reported the deprotonation of HCOOH to H^+ at the Cu(1 1 0) and Cu(1 0 0) coordination sites [61,68] whereas, this is not the case at the Cu(1 1 1) surface where the existence of atomic oxygen is critical for formate-formation. In order to elucidate the reaction mechanism for better understanding of the interaction of Cu catalysts with FA in terms of reactivity and structural sensitivity, there is need to understand the kinetics of FA-decomposition and H_2 formation; several experimental studies, lack adequate systemic theories to provide the required insights as regards FA-decomposition on Cu surfaces. Most proposals/elementary steps involved in the decomposition process are similar to those of methanol synthesis and WGS reactions in terms of their similar reaction pathway. The work of Sanni et al. [24] gave a plausible reaction scheme as mechanism for FA decomposition where the reaction simply occurs between stable copper catalysts at varied concentrations which are supported on a tertiary amine which helps to disallow the early contamination of Cu thus extending its service life. Hence, the kinetics of the process can dwell on the dehydrogenation step rather than the CO-production step which stimulates catalyst poisoning. Furthermore, efforts can be made to concentrate the FA attachment to copper catalyst at coordination sites such as Cu(1 0 0), Cu(1 1 0) and Cu(2 1 1) along the ×, y, z planes while being anchored on special supports that can extend its service life thus inhibiting the dehydration step. Previous experimental kinetic studies and micro-kinetic modelling of FA-decomposition, show that the formate formed on the Cu [69] and Pt active sites [70] proceed via a carboxyl (COOH)-mediated pathway but this route can drastically reduce the quantity of H_2 produced as compared to when the process is routed via the formate formation step hence, the need to control the reaction at optimal conditions where these sites are created by merely manipulating the process conditions rather than focusing on tweaking the adherence of HCOOH to the active sites of the Cu-catalyst. Since it is quite difficult to restrict or maintain FA decomposition to the active sites of the catalysts, the knowledge gained from the proposed mechanisms will help understand-better, what happens at the optimal conditions and what they seem to offer when the best results are obtained. The proposal here is to optimize the process conditions by varying catalyst size, pH, concentration and reaction time at a

uniform reaction temperature; this will optimize the FA-decomposition towards high hydrogen yield. In essence, when these catalysts are further examined for their structural sensitivities and coordination sites/numbers, it might be interesting to find that there may be newly created active sites that are yet to be discovered in literature since Cu is known to exhibit variable oxidation states.

Influencers/Supports for catalytic formic acid decomposition reactions

The most pressing challenge in catalyst synthesis is the attainment of highly stable, non-sintering and non-leaching substances with well-defined composition and size/shape-controlled nanoparticles. The influence of large surface area to volume ratio is one of the greatest features of these nano-metals. For a reaction that is morphologically sensitive, catalyst-sizes become the controlling factors owing to their predictive impacts on the surface morphology and electronic/sub-atomic oxidation states of the metals, hence, the need for catalyst-supports for improved results. For catalytic processes that largely depend on harsh operating conditions, catalyst-supports become necessary because, sintering and/or leaching of surface bound nano-metals bring about a decrease in the activity and unspent life of the catalysts made from them [71]. The FA-decomposition described by Carner et al. [71] involves the use of wet impregnation method to synthesize titanium II oxide nano-fines which served as anchor for PdCoNi alloy (three-in-one nano-alloy), after which they were simultaneously reduced to their metals. Furthermore, in order to enhance their stability to heat and leaching, the atomic-layer deposition (ALD) method was employed as a means of nurturing and dispersing silver oxide layers within the superficial PdCoNi, thus giving rise to (PdCoNi/TiO_2-ALD-SiO_2-TiO_2); the resulting nano-alloy (PdCoNi supported on TiO_2) appeared crystalline and sized 3.52 nm. The performance of the PdCoNi/TiO_2-ALD-SiO_2-TiO_2 catalyst was measured in terms of its

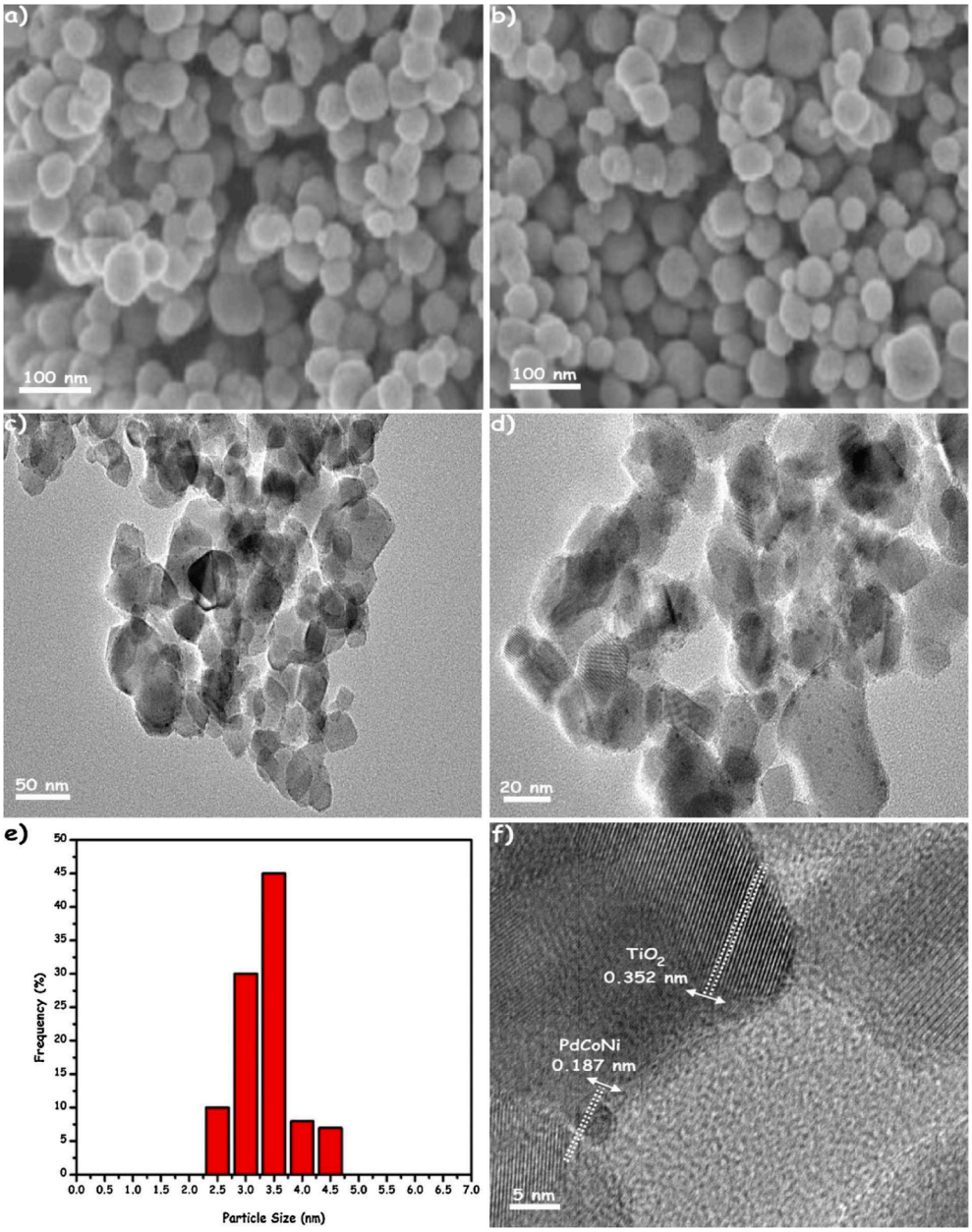

Fig. 3. a-f: a-b. FESEM morphology of $Pd_{0.60}Co_{0.18}Ni_{0.22}/TiO_2$ for different sections of the sample taken from different regions, c-d. BFTEM morphology/magnifications of $Pd_{0.60}Co_{0.18}Ni_{0.22}/TiO_2$, e. Histogram of $Pd_{0.60}Co_{0.18}Ni_{0.22}/TiO_2$ catalyst-size f. HRTEM of $Pd_{0.60}Co_{0.18}Ni_{0.22}/TiO_2$. .
Adopted from [71]

selectivity, activity and oxidative/thermal stability during the catalytic dehydrogenation stage; the hybrid catalyst-support adopted here is similar to that in ref. [72]. Formic acid (FA) is a prospective parent material for producing hydrogen [13], however, the percentage composition of hydrogen in the compound is only approximately 4%, hence, large volumes of the organic compound are required if high volumes of hydrogen are desired. According to [13], the dehydrogenation reaction occurred at room temperature with a turn over frequency of 207 mol H_2/mol metal*h and the catalyst selectivity was > 99% at near-complete conversion. They found that the catalyst-support helped to preserve the service-life by about 20 times i.e., at the 20th time of catalyst reuse, the catalyst still retained its reactivity and inherent abilities in terms of selectivity, conversion and stability, whereas, the non-anchored PdCoNi/TiO catalyst had completely lost its potency under such conditions. Sadovskaya et al. [73] developed a hybrid vanadia-titania oxide hybrid catalyst with metallic ratio of 1:13 respectively, and a specific surface area of 54 m^2/g; this is similar to the surface composition of the hybrid catalyst of the monolayer atom adopted in ref. [72] that had an average density of $8.9*10^{18}$ atoms/m^2, which was formed by first dissolving anatase titanium oxide in a solution of vanadyl oxalate (VOC_2O_4) and subsequently drying the resulting mixture in air for 12 h and calcining it at 110–450 °C for 4 h. Liu et al. [74] produced a Pd-Au alloy as catalyst for hydrogen production. Although the Au catalyst did not influence hydrogen production, they added that, it rather prevented any possible adsorption of the produced hydrogen atom, which was subsequently converted to hydrogen molecule. Fig. 3 a-f shows different views of a sample Pd-Co-Ni-TiO_2 catalyst morphology as obtained from SEM.

Zavras et al. [75] used the concept of changing the environment/reaction system at a metal centre/catalyst surface to stimulate activity/reactivity. Formic acid was the adopted raw material for synthetic hydrogen production. In their work, gas phase experiments were combined with DFT calculations as a way of examining how a binuclear silver hydride ion (AgH^+) can be manipulated using choice phosphate ligands which initiate hydride protonation and in turn liberate H_2 gas (Fig. 4). According to them, this is a very crucial step, because the decomposition of formic acid is almost impossible without ligands. Also, spectroscopic characterization of the AgH^+ shows that the ionic hydride and its ligated variants can be easily formed when needed.

Catalyst selectivity and activity

Several homogeneous catalysts have been adopted for formic acid decomposition reactions, however, one of the most recent findings by Sanni et al. [24] puts forth copper-triethanol amine system as a promising catalyst-support system for high FA conversions of about 82.7%. Also, owing to the rising research interests in establishing the mechanisms/kinetics for formic acid decomposition, a homogeneous kinetic model for catalytic-formic acid decomposition was proposed. Several other catalysts have been adopted for formic acid decomposition, but most of them are heterogeneous in kind. Despite the fact that the alloying of transition metals with noble metals is one good and ideal method of obtaining responsive and desirable catalytic FA-decomposition efficiencies, the involvement of heteroatoms makes the entire process somewhat expensive [24]. The folding, doping or encapsulation of sample metal-blends such as palladium and gold (a noble and inert element) for use as catalytic-decomposers of FA, have shown high levels of activity and selectivity for H_2 owing to the high rate of conversion obtained as compared with the H_2 yield when pure forms of the metals are used [76,77]. According to Allison and Bond [78], alloys of palladium and gold form a serial-continuous face centred cubic structure in their liquefied state which makes them a good blend for

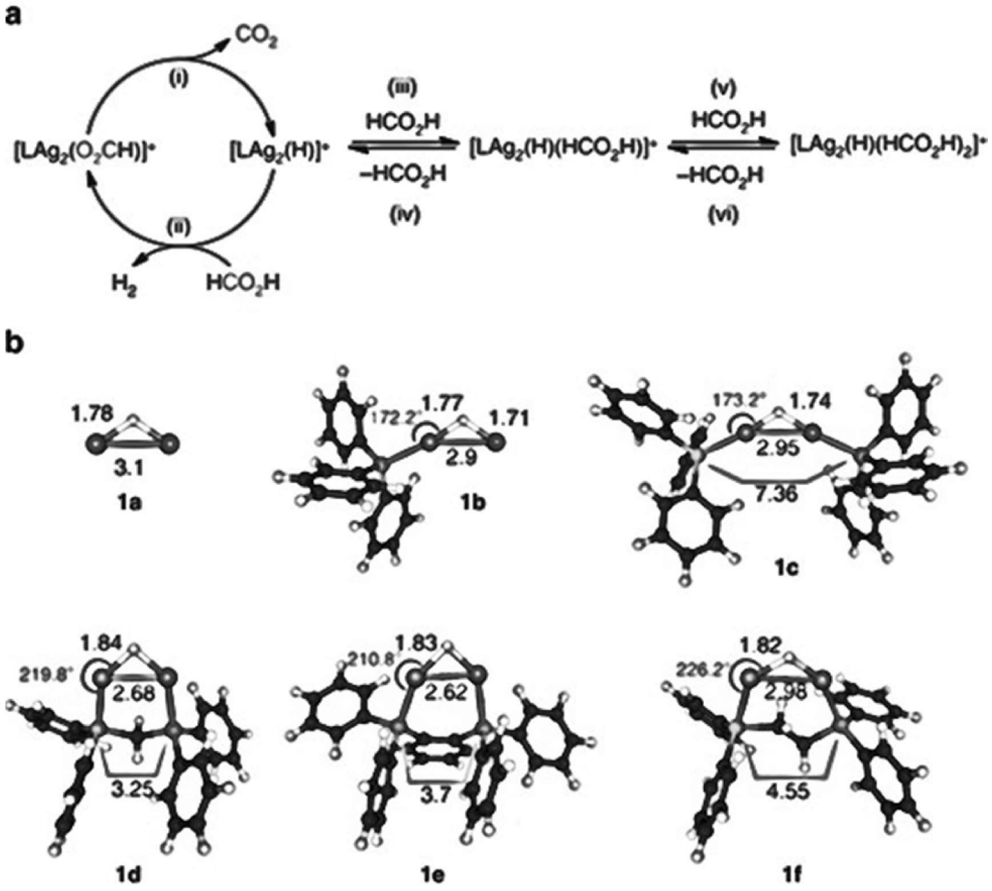

Fig. 4. a-b: Ligated silver hydride ion and its decarboxylation/dehydrogenation of formic: **a.** catalytic process cycle involving (i) the decarboxylation of $[LAg_2(O_2CH)]^+$ through collision-induced dissociation (CID) to give $[LAg_2(H)]^+$ (ii) ionic reaction of $[LAg_2(H)]^+$ to give $[LAg_2(O_2CH)]^+$ (iii) ionic combination of $[LAg_2(H)]^+$. (iv), CID of $[LAg_2(H)(HO_2CH)]^+$ to reproduce $[LAg_2(H)]^+$ (v) molecular combination of $[LAg_2(H)(HO_2CH)]^+$ and HO_2CH to give $[LAg_2(H)(HO_2CH)_2]^+$ (vi) CID of $[LAg_2(H)(HO_2CH)_2]^+$ to produce the $[LAg_2(H)(HO_2CH)]^+$.**b.** results from the most stable-structures examined: 1a-f. The DFT hybrid functional B3LYP was used alongside def2-TZVP AO as basis for all atoms and with their corresponding relativistic effective Ag-atoms core potential. Bond distances are illustrated with Å (black) and P–Ag–H bond angles in degrees (red). Adopted from Zavras et al. [75].

hydrogen synthesis. Fig. 5a-k shows the comingling of HCOOH and hydrogen atoms/molecule on a sample $Pd_{22}Au_{33}$ catalyst cluster.

The activity of PdCoNi/TiO_2-ALD-SiO_2 catalyst was examined by Caner et al. [71] during formic acid decomposition; they accounted for the performance of the catalyst by constantly monitoring the volumetric-hydrogen evolution using gas displacement technology as discussed in previous works [79–92]; in testing the catalyst's performance, the weight of the catalyst reaction flask was monitored per time. In recent times, pure separate atoms of Au and Pd, as well as Pd-Au core shells and Au-Pd core-shells were synthesized as catalytic decomposers of formic acid. The volume of hydrogen produced from the reactions catalysed by the last three catalysts were obtained in the following order: 100 mL in 600 min, 230 mL in 150 min and 200 mL in 50 min, respectively. The results revealed the increased catalytic activities as well as product (H_2) selectivity of the catalysts for FA [93]; these results are also supported by results obtained by other investigators [87,94–99]. Catalyst-orientation can be in several categories including single crystals [100–102] and bulk forms [103], as supports/anchors [104–106], organic complexes of metals [107,108] and metallic salts [109]. Noble metals only have the capacity to catalyse the dehydrogenation step of formic acid decomposition while base metals and their oxides are useful for the dehydration and dehydrogenation steps [104]; this justifies the idea of catalyst-hybridization in order to take advantage of, as well as maximize the catalytic potential of each class/type of catalyst. However, based on the work of Sanni et al. [24], it is obvious that the Cu-tertiary amine system adopted, has the ability to overcome these odds since the dehydrogenation step induced by noble metal-catalysts takes advantage of the intermediate formates/complexes formed at the dehydrogenation stage [100,105]. According to Silbaugh et al. [106] monodentate formate is a key intermediate product of formic acid decomposition that is further converted to bidentate formate; this reaction is reversible in nature which explains the tendency for re-establishing the system's equilibrium. The thermochemical analyses of the decomposition of HCOOH on sample-facets of Au, Ag, Co, Cu, Ni, Os, Pt, Pd, Rh and Ru catalysts have been investigated [18]. The study discussed the use of DFT in examining the mechanisms of HOOH-decomposition to give HCOO* via surface intermediates or the release of the carboxyl group via COOH*-surface intermediate. Based on the findings, the adsorption of HCOOH at the water-removal stage helps to disintegrate either the C–H bond to form COOH* or the O–H bond to form HCOO*. Thereafter, cleavage and evolution of the remaining proton and CO_2 take place respectively. A systemic analysis of bulk-metal catalyst-activity in HCOOH decomposition was carried out by monitoring parameters such as surface composition of metals, number of catalyst-active-sites, type of surface intermediates formed, formic acid adsorption equilibrium, Density Functional Theory -Thermal Dynamics (DFT-TD) and reaction rates at steady state [103]. According to their hypothesis, all the catalysts provided evidence of CO_2 and CO formation during the dehydration and dehydrogenation steps of surface HCOO* species, respectively. It was also reported that the TD-Drifts revealed that the surface HCOO* may be mono- or bi- dentate in kind, depending on the metal-catalyst adopted. Furthermore, they observed that there was no correlation between the resulting gas-ratio (i.e. CO_2 to CO ratio) and the nature of surface formates formed for each catalyst. Based on HCOO* decomposition rates, the following list was established in increasing order of catalyst-performance: Rh < Fe < Ag < Ni < Au < Co < Pd < Cu < Pt and, these were found to bear a poor correlation with the Turn over Frequencies (ToF) at steady-state. The work of Zhong et al. [110] involves the use of a Pd heterogeneous catalyst for the catalytic dehydrogenation of HCOOH, while Li and Xu [111] also adopted a nano-catalyst in synthesizing high pressure hydrogen from formic acid.

Table 2 contains the rates of formation (W_{st}) of CO and CO_2 measured at steady state (i.e. for varying %volume of hydrogen produced) for different experimental runs at 120 and 140 °C. The CO conversion (X%) and Catalyst Selectivity for CO (S_{Co}) are also shown as obtained from the experiment. Based on the results, it can be inferred that the rate of decomposition of HCOOH is less dependent on acid concentration but on %vol of H_2O formed. Looking at the data generated for experimental runs 1 and 2. For zero %water volume, the transformation rate/conversion and selectivity only varied slightly within the range of 10–13% and 78–76%, respectively for a change of 2.4–1.3 HCOOH-acid concentration at 120 °C. Comparing the %vol of water in runs 3–5, the conversion dropped from 9 to 5% with the CO selectivity S_{CO} dropping to as low as 47%; the rate of formation of CO_2 also dropped from 0.27 to 0.24, hence, CO_2 selectivity shows an indirect variation

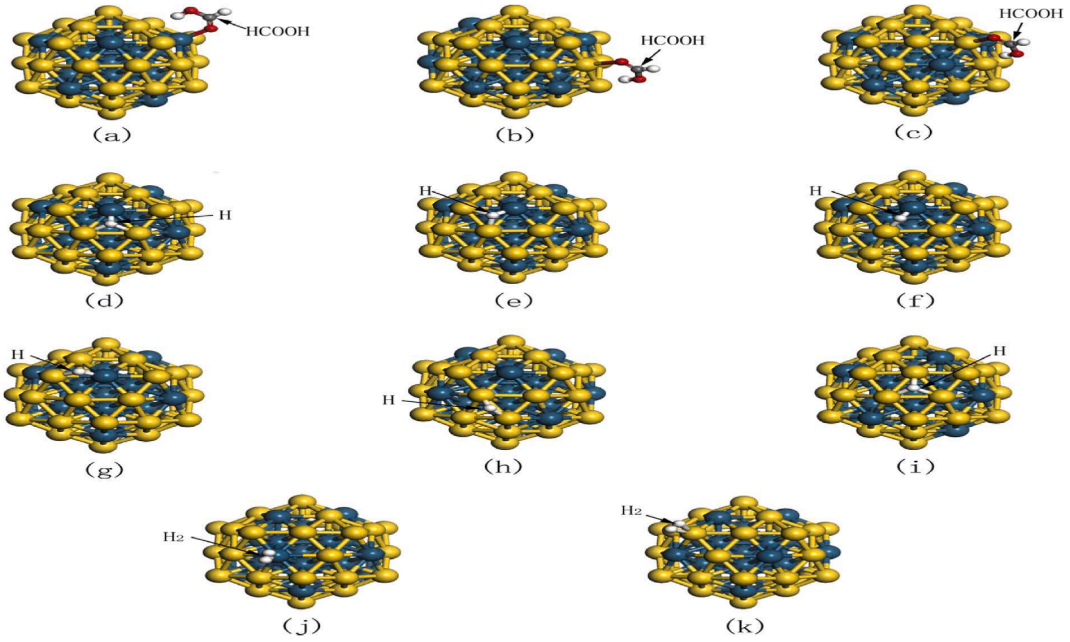

Fig. 5. (a-c) Plausible active sites for adsorbing reactants (HCOOH) or product (H_2), (d–i) Hydrogen atom and (j-k) Attached hydrogen molecule (H_2) on a sample $Pd_{22}Au_{33}$ cluster. .
Adopted from [74]

Table 2
Steady State Formic Acid-Decomposition Data for Different experimental runs.

No	T^a, S	Conc.	%vol		X%	Wst * 10^9		S_{Co}%
		HCOOH	H_2O	O_2		CO	CO_2	CO
T @ 120 °C								
1	0.77	2.4	0	20	10	1.34	0.38	78
2	0.79	1.3	0	20	13	1.26	0.4	76
3	0.45	2.3	3.8	20	9	0.59	0.29	67
4	0.50	1.4	3.8	20	12	0.47	0.27	64
5	0.44	2.2	9.5	20	6	0.29	0.24	55
6	0.46	2.3	14.5	20	5	0.22	0.24	47
T @ 140 °C								
7	1.94	1.8	0	20	25	8.3	1.3	86
8	0.56	2.0	9.8	20	20	1.8	0.51	78
9	0.46	1.8	15.0	20	27	1.8	0.5	78
10	0.49	1.7	17.0	20	23	1.5	0.55	73

T^a = contact time, Conc. = concentration, Wst.
Source: Sadovskaya et al. [73].

with the amount of water recovered. For water concentration in the range of 0–14.5%, the rate of CO formation dropped by 6 times at 120 °C, while the S_{Co} dropped by about 30%. When the reaction temperature was raised to 140 °C, the overall rate of decomposition of HCOOH and S_{Co} increased (see results obtained at 120 °C). Since water vapourizes faster at 140 °C relative to 120 °C, the effect of water vapour on the reaction at 140 ◦C is less pronounced. For a %vol H_2O of 0–15%, the rate of formation of CO dropped by 4.5. Also, the selectivity of the catalyst towards CO decreased by 10% approximately.

Because, a catalyst selectivity of less than 50% CO is poor (Table 2), the values for all 3 parameters in Fig. 6 were chosen from runs 1–3. The optimum HCOOH concentration for high CO selectivity is between 2 and 3 M for 0.44–0.45 T^a,S with respective water volumes of 3.8 and 9.5% as obtained from the dehydration steps for runs 2 and 3. An equilibrium point where S_{CO} selectivity = 77% was also established between both runs. Furthermore, in order to obtain the best results, the conditions suggested for runs 2 and 3 must be maintained. Borrowing a leaf from the observations in ref [73], while considering the very high FA-conversion obtained by Sanni et al. [24] for both theoretical and experimental hydrogen estimates, it then implies that the CO selectivity was impeded up to the 20th run by the help of the tertiary amine which served as support for the Cu-catalyst, however, CO selectivity increased after the 20^{th} run because there was an incipient drop in the catalytic activity of Cu-triethanolamine, which further resulted in the reduction in volume of hydrogen recovered for further runs. This they allotted to be caused by catalyst poisoning, pH alteration, formation of a complex, steric hindrance etc.

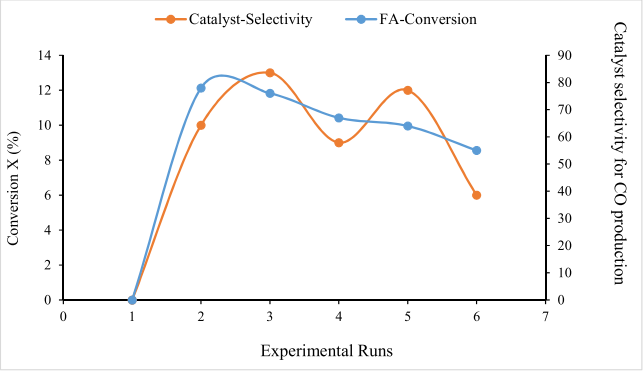

Fig. 6. Catalyst selectivity for CO vs HCOOH-Concentration and Conversion @ 120 °C.

Bond energies of reacting species in FA decomposition reactions

The catalytic-activities of single metal catalysts are enhanced when they are hybridized or alloyed. This is because of the synergistic effect offered by each of the metals in their combined form, which in turn lowers the activation energy of the reaction to give H_2. It has been reported that the superficial energy of Au is smaller than that of Pd [112], which is the reason the surface area/active sites of the hybrid catalyst is rather more-enhanced as induced by Au [113]. What this then suggests is that, for heterogeneous catalyst-composites, the wrapping material is of utmost concern i.e., it should comprise more of the more/most active metal of any two or more catalyst-options. According to Ding et al. [114], the nano-clustering nature of metallic nano-composites can be examined using a High-Resolution Transmission Electron Microscopy (HRTEM). Based on their findings, after epitaxially-growing the less active metal (Pd) on the more active metal (Au), there was a concentration gradient set up within the crystal lattice of the alloy, which further resulted in the diffusion of Au to the surface, thus annulling the lattice mismatch between both atoms. In addition, the presence of both atoms along the Long Range Ordered Plane (LROP) is approximately 1:1 which is stable below 800 K. According to Wang et al. [102] the decomposition of formic acid on Pd surface to give two moles of hydrogen atoms and one mole of CO_2 is possible within surmountable/permissible reaction constraints, however, there is need for caution since Pd has high affinity for hydrogen thus causing dissociation of the atoms and subsequent binding of the atoms to the surface of Pd; this strong hydrogen adherence makes it almost impossible for the comingling of two H atoms to form hydrogen molecule on the surface of Pd [115]. On the contrary, the adherence of hydrogen to the surface of Au is characterized by a weak bond [116] and based on the account of Yu et al. [117], the average characteristic bond-energy of hydrogen to the Au-Pd nanocluster-surface lies between the individual bond energies of both atoms. To complement the aforementioned statement, Liu et al. [73] opined that, the increased production of hydrogen from HCOOH decomposition is as a result of the weak forces of adsorption of H_2 on the Au-Pd surface.

Table 3 gives the nature of the active sites and adsorption energies of PdAu clusters to H_2, H and HCOOH; some of the species are attached to vertices, the face-/hexagonal-cubic centres, along edges, as well as bridges of the catalyst clusters. In accordance with previous discussions, the bridge, face/hexagonal centres and edges mentioned for the single and heterogeneous catalysts in ref. [73], can be likened to the different orientations exhibited by the coordination sites of copper i.e. Cu(1 1 0), Cu(1 0 1) and Cu(1 1 1) when used on catalyst supports such as triethanolamine.

Elementary steps for hydrogen formation from formic acid

HCOOH-decomposition is largely contributed by the dehydrogenation step. The overall decomposition involves two process routes: dehydrogenation and dehydration whose reaction rates are dependent on the nature/type of catalyst, system-pH as well as the reaction temperature (if not kept constant) [118]; the stoichiometric equations for the reactions are as given by (2) and (3).

Scheme A

$HCOOH \xrightarrow{Cu2+/R1R2NH2} H_2O + CO \quad \Delta G_{353\ K}$ ($\Delta G_{298\ K} = -14.9$ kJ/mol (Dehydration- initiation step) (2)

$HCOOH \xrightarrow{Cu2+/R1R2NH2} H_2 + CO_2 \ \Delta G_{353\ K}$ ($\Delta G_{298\ K} = -35.0$ kJ/mol (Dehydrogenation-initiation step) (3)

The first step is a dehydration step (2), while the second (3) is the dehydrogenation step where hydrogen is produced.

Mackay et al. [119] proposed two reaction schemes for HCOOH decomposition as presented in (4) and (5).

Table 3
Active sites and adsorption energies of HCOOH, H and H_2 on Pd_{55}, $Pd_{27}Au_{28}$ and $Pd_{22}Au_{33}$ clusters.

Species	Pd_{22}		Pd_{27}		Pd_{55}	
	Active site	Elec. Volts $*10^{-1}$	Active site	Elec. Volts	Active site	Elec. Volts
HCOOH	(a) Vertex	−8	(a) Pd	−0.7	(a) Pd	−0.66
	(b) Edge	−7.3	(b) Au vertex	−0.5	(b) Au vertex	−0.53
H	(c) Fcc	−3.13	(c) Au edge	−0.28	(c) Au edge	−0.32
	(d) Hcp	−3.10	(d) Pd_2Au fcc	−2.94	(d) $PdAu_2$fcc	−2.64
	(e) Bridge (Vertex-edge)	−3.01	(e) Pd_2Au hcp	−2.91	(e) $PdAu_2$hcp	−2.61
	(f) Bridge	−3.00	(f) $PdAu_2$ hcp	−2.63	(f) PdAu bridge (Au edge)	−2.62
H_2	(g) Vertex	−0.48	(g) PdAu bridge	−2.74	(g) PdAu bridge (A_u vertex)	−2.65
	(h) Edge	−0.51	(h) AuAu bridge	−2.5	(h) AuAu bridge (vertex-edge)	−2.42
			(i) Pd	−0.5	(i) Au_3 fcc	−2.3
			(j) Au vertex	−0.14	(j) Pd	−0.46
					(k) Au vertex	−0.16

Source: Liu et al. [73].

$$(HCOOH)H^{+} \xrightarrow{k_{H3O}^{+(Cu^{2+}/R1R2NH2)}} H_3O^{+} + CO\Delta Hr_{353}(\Delta Hr_{298} = 78\ kJ/mol,\ protonation - final\ step) \quad (4)$$

$$(HCOOH)H^{+} \xrightarrow{k_{HCO}^{+(Cu^{2+}/R1R2NH2)}} HCO^{+} + H_2O\Delta Hr_{353}(\Delta Hr_{298} = 181kJ/mol\ (Dehydration - final\ step) \quad (5)$$

If it is assumed that all four reactions are important steps in formic acid decomposition, then, in combining those two schools of thought, one can see all four steps as being very important to the hydrogen formation step, hence the proposed scheme of elementary steps for HCOOH decomposition is in the order of (4–5 or 2–3). The distribution ratio of HCO^+:H_3O^+ is 7:3 and the reactions in equations (4)–(5) show that the decomposition of protonated metastable ions of HCOOH give hydroxonium and formyl ions [120,121]. The difference in heat of reaction values for both steps was reported to have some measure of thermochemical variations during their product formation steps. The percentage composition of the products of the reactions in equations (2)–(5) are as shown in Table 4a. However, the heat of reaction is obviously lowered alongside the estimated ΔG at 353 K; more explanation is given on this in section Structural forms and activation energies of reactions at the active sites of copper considering the active sites of copper.

Table 4a
Energy requirement for the protonation and dehydration steps of FA decomposition.

Temperature, K	Products (%)	
	$H_3O^+ + CO$	$HCO^+ + H_2O$
298	60	40
1000	40	60
This work		
353	82.2	17.8

Adapted from ref. [121].

Other supplementary reactions proposed by Sekiguchi et al. [121] for FA decomposition can be mimicked for the Cu-triethanolamine-FA system:

$$CuR1R2NH_2^{+} + HCOOH \xrightarrow{k_1} [HCOOH]H \quad (6)$$

$$(HCOOH)H+ \xrightarrow{k_2} H_3O^{+} + CO \quad (7)$$

$$(HCOOH)H+ \xrightarrow{k_3} HCO+ + H_2O \quad (8)$$

$$H_3O^{+} + HCOOH \xrightarrow{k_4} [HCOOH]H^{+} + H_2O \quad (9)$$

$$HCO^{+} + HCOOH \xrightarrow{k_5} [HCOOH]H^{+} + CO \quad (10)$$

Scheme B

$$Cu - R1R2NH_2 + HCOOH^{k_6} \rightarrow Cu - R1R2NH_2 + HCOOH^{+}\Delta Hr = 137\ kJmol^{-1}(dehydration) \quad (11)$$

$$HCO^{+} + HCOOH^{k_7} \rightarrow H_2 + Cu - R1R2NH_2 + HCOO^{+}(final\ step)\ \Delta Hr = 49\ kJmol^{-1}(dehydrogenation) \quad (12)$$

$$ToF = \frac{P_{atmospheric}V_{gas}}{\frac{RT}{2*n_{Cu}t}} \quad (13)$$

Where:

$P_{atmospheric}$ = atmospheric pressure in N/m^2 = (101325 Pa),

V_{gas} = generated volume of $H_2 - CO_2$ gas (815 mL/2 = 407.5 mL) at half-life of the gas generation,

R = universal gas constant (8.3145 m^3 Pa mol^{-1} K^{-1}),

T = reaction temperature (333 K),

n_{Cu} = total mole number of Cu atoms in catalyst (0.8315*1; obtained from Table 4), and t is the time of half-completion of gas generation (180 min).

$$HCOOH \xrightarrow{R1R2-NH2/Cu2+} CO_2 + H_2 \quad (14)$$

The energy difference of the dehydration step at 298 K as given in equation (4) is expected to be less than the energy requirement of equation 8 (whose value was not reported), this is evident due to the difference in the dehydrogenation steps of schemes A and B as seen in equations (4) and (12), respectively, giving a change of 29 $kJmol^{-1}$. Comparing the total heat of reaction for the dehydrogenation step in scheme A (heat-summation of equations 2, initiation step and 4, final step = i.e. (-35 + 78) = 43 $kJmol^{-1}$) to that of the final step of scheme B i.e. equation (11) (49 $kJmol^{-1}$), it is obvious that the latter (dehydrogenation step- scheme B) gives more energy consumption than the former (dehydrogenation step- scheme A) with the energy difference of both schemes' being 6 $kJmol^{-1}$. Also, the quantity of heat required for the dehydration step is far higher than that required for the dehydrogenation step. This then justifies the reason why some reactions are initiated at higher temperatures depending on the ability of the catalyst to alter the reaction rate or impede the dehydration step, so that most of the energy supplied to the system is not used in producing water and CO, which reduces the tendency for hydrogen release from FA. When scheme A is critically examined, the reaction in 5 then looks to comprise of the series of elementary steps shown in scheme B's (reactions (6)–(12)) dehydrogenation-step, that is, both schemes seem to have similar characteristics/features despite the difference in the heat of dehydrogenation (i.e. 6 $kJmol^{-1}$) of both schemes, which may have been stimulated by the nature of the reactions in the schemes, variation in catalyst type, support(s) and process conditions. Table 4b gives a summary of the metallic cations and conditions for exemplifying the FA dehydrogenation steps explained in scheme B.

The average ToF of hydrogen gas produced from FA dehydrogenation reactions, as well as the estimated activation energies of the

Table 4b
Summary of some metallic cations alongside Cu^{2+}/R1R2NH_2 conditions responsible for the HCOOH decomposition.

Cation	Radical/ atom	Difference in proton affinity $\Delta P_{r.aff}$ (kJmol^{-1})	Method of synthesis
HCl^+	I	138.8	Electron ionization of ammonium iodide
H_2Cl^+	HCl	185.1	Chemical ionization of NH_4Cl to H_2Cl^+
CH_5^+	CH_4	198.5	Chemical ionization
HCO_2^+	CO_2	201.5	Electron ionization of HCOOH
HCl	Cl	228.4	Electron ionization of NH_4Cl
Cu^{2+}	R1R2NH_2	Not measured	Chemical vapour deposition

Adopted from Sekiguchi et al. [121]; Lias et al. [122].
$\Delta P_{r.aff} = \Delta P_{r.aff}$ (Metal) - $\Delta P_{r.aff}$ (formic acid). All values have uncertainties in the region of 10 kJmol^{-1} while $\Delta P_{r.aff}$ (HCOOH) = 228.4 kJmol^{-1}.
M = metallic cation and MH^+ = metallic composite.

reactions at different temperatures, for different catalysts, are documented in Table 5.

Table 6 compares the results of the estimated ToFs as obtained for some catalysts and that of the referred Cu-tertiary amine system synthesized by Sanni et al. [24]. The data shows that the only single catalysts that performed better than the Sanni et al. [24] catalyst system, are cobalt and platinum with ToFs of 3000 and 980 s^{-1} respectively. The Estimated ToFs of the catalyst systems in Table 6, as well as that of the 1 M CuNP-tertiary amine system, were obtained from (13). The value of the Turn over Frequency (ToF) estimated here is an apparent ToF which is dependent on the number of Cu atoms in the CuNP-catalyst, and was estimated based on the half-life of the gas (H_2) produced.

Table 5
Catalytic performance of different catalysts used in the dehydrogenation of formic acid.

Catalyst	T (K)	ToF initial (h^{-1})	Con. (%)	Ea kJ mol-1	Ref.
$Pd_{60}Au_{40}$/ZrSBA-15-AP	298	1185	95	42.5	[123]
Pd/CNx	298	639	98	48.8	[124]
Ag@Pd/C	298	157	43	–	[82]
AgPd/C	298	274	46	22.0	[125]
AuPd/C	298	41	24	28.0	[86]
CoAuPd/C	298	54	91	–	[97]
NiAuPd/C	298	20	73	–	[126]
AgAuPd/rGO	298	95	100	–	[127]
CoAuPd/r-GO	298	63	51	–	[128]
CoAuPd/DNA-rGO	298	130	96	–	[128]
AuPd/N-mrGO	298	39	93	–	[83]
Au@Pd/N-mrGO	298	111	98	–	[83]
AuPd/N-rGO	298	17	57	–	[129]
AuPd-CeO_2/N-rGO	298	68	98	–	[129]
AuPd/ZIF-8-rGO	298	532	83	–	[99]
AuPd-MnOx/ZIF-8-rGO	298	764	94	–	[99]
PdAg-MnOx/N-SiO_2	298	482	99	72.4	[88]
CrAuPd/N-SiO_2	298	707	87	49.8	[89]
PdAu/N-SiO_2	298	164	76	26.2	[87]
PdAu-MnO_x/N-SiO_2	298	981	92	26.2	[87]
AgPd@MIL-100 (Fe)	298	58	37	–	[130]
Pd/SBA-15-NH_2	298	127	28	–	[131]
PdNiAg	323	85	94	–	[90]
SR13 FHL strain	310	1228	–	–	[38]
PdAu-MnO_x/N-SiO_2	298	78.5	92	–	[132]
MnO_2 & MnO_x/RGO	298	0.0003–0.003	–	–	[133]
Au-ZrO_2	325	1590	–	–	[81]
PdAg-MnO_x/N-SiO_2	363	1400	99	–	[88]
CuI	368	1.8	28 mmol	–	[134]
$Cu(OAc)_2$	363	0.98	28 mmol	–	[134]
$IrNaO_2CH$	363	964	99	–	[134]
Ru	36–400	964	12.7 mmol	–	[108]
Pd^{2+}/C	353	7,256	98	–	[135]
Fe-pincer/$LiBF_4$	298	247	2.9 mmol	–	[136]

Table 6
Number of Active sites (Ns), Steady-state, ToF for homogeneous catalysts at 250 °C and the Cu-amine catalyst synthesized at 60 °C.

Catalyst (μmol/g)	Number of active sites (Ns)	HCOOH Activity 250 °C (μmol/g•s)	TOF 250 (°C/s)
Co	$3.1*10^1$	$9.3*10^{-2}$	$3.0*10^3$
Fe	$1.8*10^2$	$4.0*10^0$	$2.2*10^{-2}$
Ag	$7.6*10^0$	$3.0*10^0$	$3.9*10^{-1}$
Au	$5.2*10^1$	$4.0*10^1$	$7.7*10^{-1}$
Ni	$1.6*10^2$	$1.5*10^3$	$9.3*10^0$
Rh	$1.5*10^1$	$4.8*10^1$	$3.3*10^0$
Pd	$9.9*10^1$	$1.6*10^2$	$1.6*10^1$
Cu	$1.6*10^1$	$5.2*10^1$	$3.2*10^1$
Pt	$1.9*10^1$	$1.8*10^3$	$9.8*10^2$
CuNP-amine	$4.35*10^0$	ND	$358.8*10^0$ @ 60 °C [24]

Source: Adopted from [24,103].

Based on the sizes of the CuNPs obtained, the best CuNPs were those with an average particle size of 1.5 nm size. Particle size, pH, concentration and reaction time were recounted as variables that affected the performance of the CuNP-tertiary amine system (Fig. 7). The loop in Fig. 8, shows the variation of Cu loading, pH and concentration. Knowing the value of any two of the three variables shown in the loop, will help ascertain what the value of the third variable would be without the need for any form of experimentation. Also, the optimum pH, concentration and particle size for obtaining a theoretical conversion of 100% and an actual conversion of 82.7% were estimated to be 3.19, 1 M and 1.5 nm, respectively (Fig. 8a). Fig. 8b is a profile of the variation of partial pressure with time for the Cu-triethanolamine system.

According to the Differential Method of Analysis (DMA) established by Sanni et al. [24], for a single catalyst-support system, the estimated order of the reaction for FA-decomposition using the CuNP-tertiary amine system, is a first-order type with intercept –RTlnk = 0.004091 (Fig. 9) and a corresponding rate constant or k-value of 1.0041 s^{-1}. They also mentioned that, the methods used in establishing the dehydrogenation kinetics can be adopted for other single catalyst systems, whereas, for multi-catalyst or heterogeneous catalyst-support systems, the approach discussed might require some form of modification owing to the complex nature of such systems. Based on their explanations, it is the first study that adopted the differential method of analysis to establish the dehydrogenation kinetics of FA in terms of partial pressures of the species in the system.

Exploring the plausible reaction pathways and copper surfaces for FA-Decomposition

Unlike the case of Au catalyst used in FA decomposition, where three pathways i.e. HCOO (formate), COOH (carboxyl) and HCO (formyl) are possible as illustrated in Fig. 10, the HCO intermediate is not a feasible pathway for the case of Cu-FA decomposition, because, the HCO pathway occurs as a result of dehydroxylation of HCOOH by Au catalyst, which has higher activation energy compared to those of HCOO and COOH pathways, hence, the HCOO and COOH pathways are the only pathways considered for Cu-catalysed FA reactions.

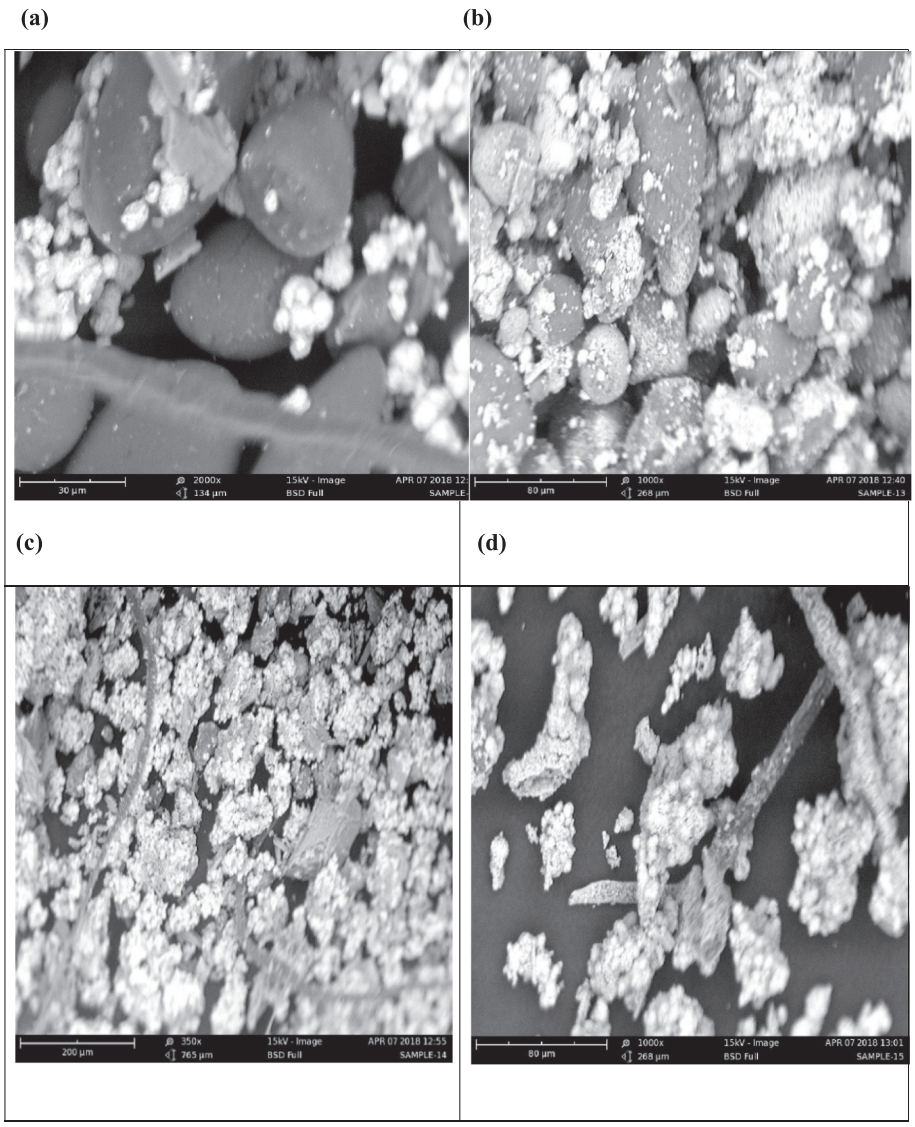

Fig. 7. SEM images of the: a. 0.6 M, b. 0.8 M, d. 1.0 M and d. 1.2 M CuNPs. Adopted from Sanni et al. [24].

Structural forms and activation energies of reactions at the active sites of copper

Adsorption configurations of five intermediates have been extensively studied on three Cu facets as illustrated in Fig. 11a and b. Hydrogen atom selectively binds at the three fold Face Centred Cubic (fcc) site of Cu(1 1 1) with an energy of −2.26 eV, while the binding energy at the Cu(1 0 0) site is lower by −0.01 ev at its readily available four-fold site. According to the investigation, the 3-fold fcc site nearest to the edge, is the preferred end for H-adsorption at the Cu(2 1 1) site; there is also a lower H-binding energy of −2.38 eV at the Cu(1 0 0) site. The CO_2 released during the decomposition was seen to exhibit null preference for the three Cu facets, thus retaining its gas-phase linear geometry, which is characterized by a weaker binding energy i.e., −0.1 eV that is suggestive of physiosorption on the Cu-surface.

Also, Li et al. [50] mentioned that the carboxyl group binds to two Cu atoms at the Cu(1 1 1) surface via its free carbon and oxygen atoms, whose C–O bond almost runs parallel to the O–H bond pointing to the surface with an estimated bond energy of −1.44 eV; this type of adsorption is also similar to what was observed at the Cu(2 1 1) step edge-surface. At the Cu(1 0 0) facet, the COOH group attaches to two opposite bridge sites in a square surrounding a hollow site. COOH has stronger affinity for Cu(1 0 0) and Cu(2 1 1) sites as compared to Cu(1 1 1) by 0.30 and 0.46 eV energy differences, respectively. On all three coordinates, formate attaches in a bidentate configuration with its oxygen atoms bound to adjacent top sites, whereas, step-edge top sites are preferable for HCOO-attachment to the Cu(2 1 1) site; the approximate binding energy of HCOO at the Cu(1 1 1), Cu(1 0 0), and Cu(2 1 1) sites are −2.57, −2.95, and −3.17 eV, respectively. FA binds to the top site of all three surfaces of Cu with its free oxygen atom. While its C–H bond points away from the site, the O–H bond points inwards. At the Cu(2 1 1) surface, HCOOH attaches itself to the top-side of the step edge during the reaction and the O–H bond is seen pointing at the step-foot atoms positioned on the terrace. The bond energy of FA increases in the order of Cu(1 1 1) < Cu(1 0 0) < Cu(2 1 1), with corresponding energies of −0.16, −0.32, and −0.47 eV at all Cu-surfaces respectively. CO_2 is also physically adsorbed and both intermediate pathways tend to attach to the step edge of Cu(2 1 1), thus giving binding energies in decreasing order of magnitude at all sites i.e. Cu(2 1 1) > Cu(1 0 0) > Cu(1 1 1); this was found to be in support of the notion that adsorbates exhibit higher binding strengths for unoccupied/open facets.

The profiles of the transition states of each minimum energy path is shown in Fig. 11b. Tentatively, HCO formation during dehydroxylation of FA on Cu(1 1 1) has a binding energy and activation energy of 1.10 eV and 1.52 eV [31] respectively, which triples the activation energy of HCOO (formate) formation from FA; this value is 0.39 eV higher than the value for the carboxyl path (COOH) formation from HCOOH at the Cu

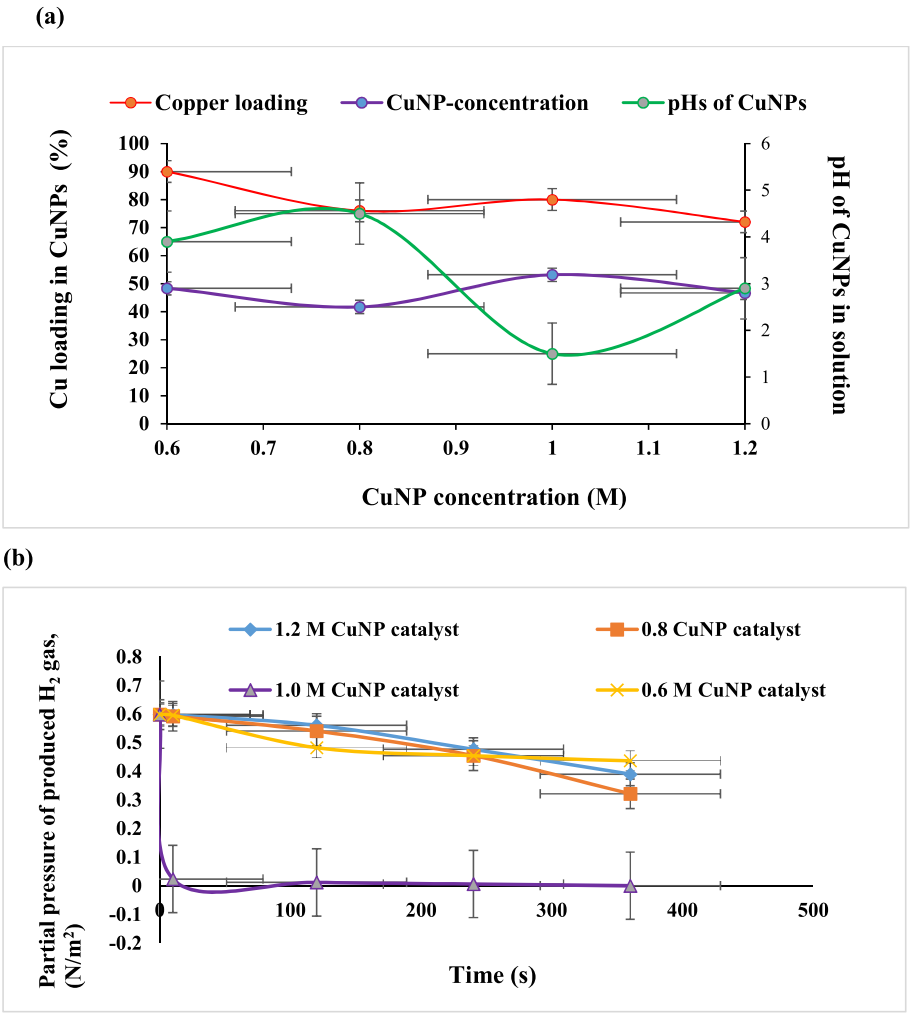

Fig. 8. a. % composition of copper in CuNP, pH of CuNPs solution vs concentration, b. Variation of Partial pressure of the H_2 gas with time. Source: Sanni et al. [24].

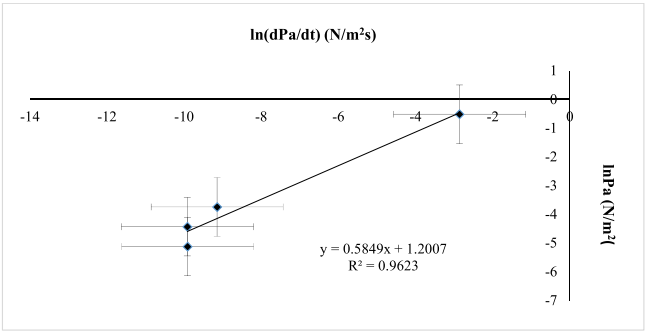

Fig. 9. Plot of ln(dpa/dt) vs ln(pa). .
Adopted from [24]

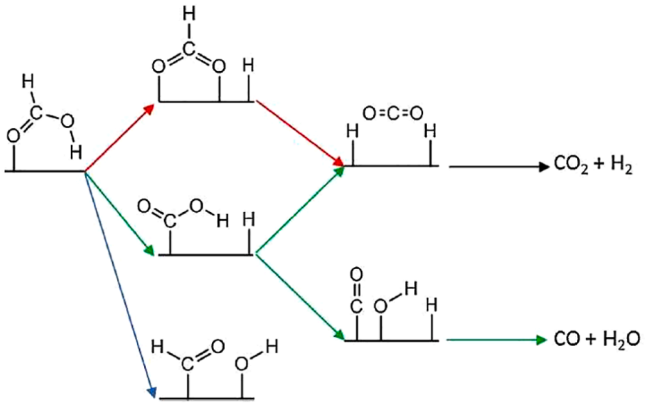

Fig. 10. Pathways of FA decomposition for reaction catalysed by Cu catalysts; the red arrows signify HCOO pathway; green arrows depict COOH pathway; the blue arrow shows the HCO pathway. The shared desorption step for H_2 production for the HCOO and COOH pathways is indicated by the black arrow. Adopted from Li et al. [50].

(1 1 1) site, hence, a true confirmation that FA decomposition cannot occur via the formation of HCO as intermediate. HCO can only give rise to CO production, whereas, there is substantial evidence that CO_2 and H_2 are the only feasible products of FA-decomposition on Cu-catalysts [24].

During FA decomposition, the formation of formate (HCOO) proceeds with the breaking of O–H bond over bridges at the Cu(1 1 1) and Cu(1 0 0) sites, and on the step-edge at the Cu(2 1 1) surface. The reaction is exothermic with corresponding reaction energies of −0.33, −0.57 and −0.74 eV, and decreases in the following order Cu(1 1 1) > Cu (1 0 0) > Cu(2 1 1), which is caused by the higher binding strength of the formate/intermediate HCOO at the more open sites. The estimated activation energies of the weak structural sensitivity of the O–H bond at the three sites, was found to fall within the range of 0.41–0.48 eV, hence, configurations of the transition states appear similar. The C–H bond-

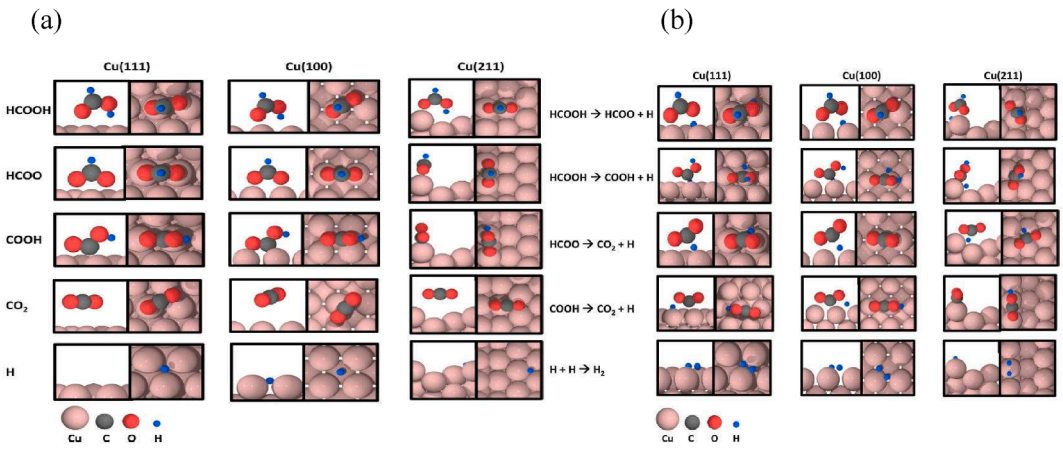

Fig. 11. a. Different configurations of reaction intermediates at the Cu(1 1 1), Cu(1 0 0) and Cu(2 1 1) facets. b. Cross-sectional and top views of transition states of the elementary steps at the Cu(1 1 1), Cu(1 0 0) and Cu(2 1 1) sites/plane. For the intermediates, the cross-section (left side) and top (right side) are as illustrated with Cu, C, O and H atoms depicted by pink, grey, red and blue spheres. Adopted from Li et al. [50].

isolation in FA to give COOH and hydrogen atom involves a rotation of the reactant molecule with the C–H bond pointing at the surface. Upon attaining the transition state, C–H bond scission may occur at the top site where COOH is absorbed via the carbon atom formed from the reaction; the atomic-H formed adheres to the closest fcc or bridge sites of the Cu (1 1 1) and Cu(1 0 0) facets, whereas, at the Cu(2 1 1) surface, C–H bond breaking occurs above the top site step-edge. After decomposing the reactant, the carboxyl group (COOH) is absorbed at the two adjacent topsides of the step edge, while hydrogen atom attaches to the hollow site of the edge. In essence, FA-decomposition via the HCOO is

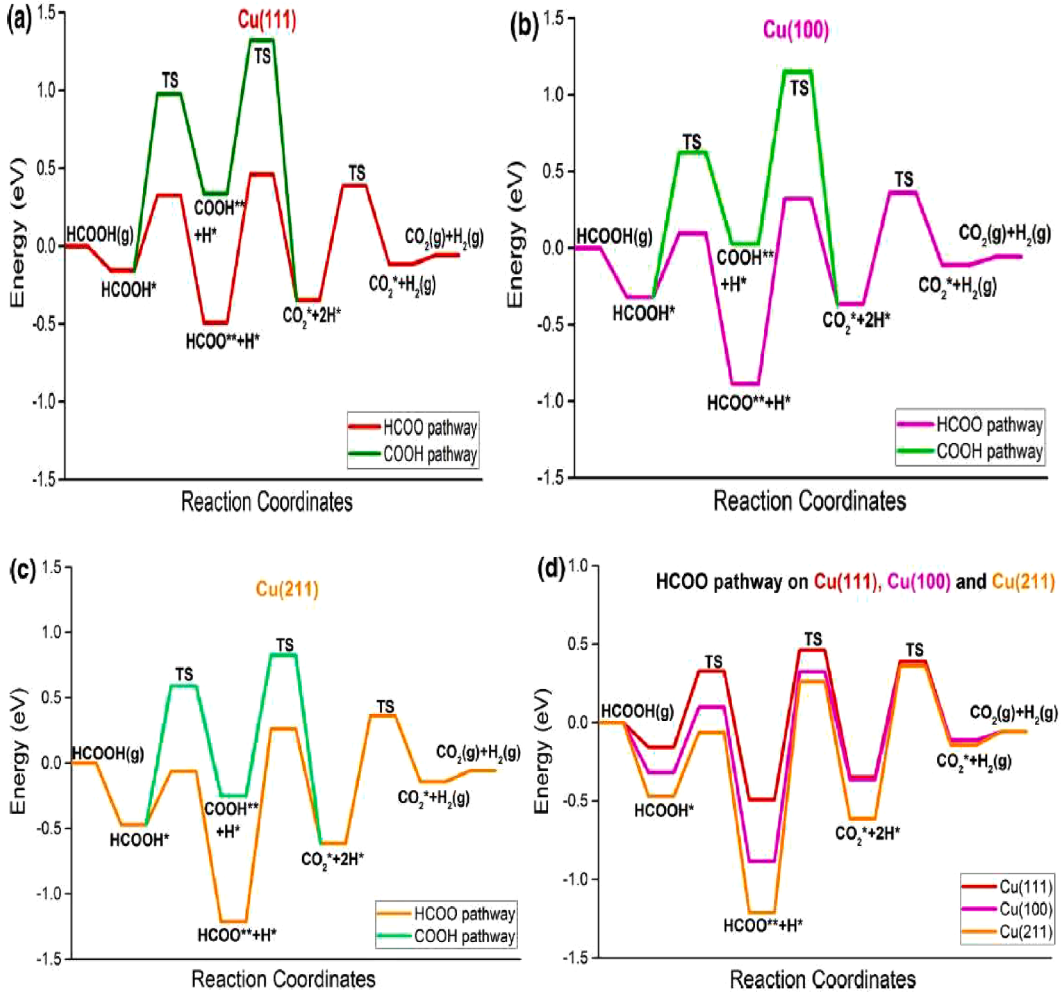

Fig. 12. Potential energy profile of FA-decomposition for the HCOO– and COOH-mediated pathways at: a. the Cu(1 1 1) surface, b. the Cu(1 0 0) surface, c. the Cu (2 1 1) surface, and d. Cu(1 1 1) surface. Adopted from Li et al. [50].

exothermic, while, it is endothermic for the COOH pathway for all three surfaces owing to the heat/energy-gain during the adsorption of COOH relative to HCOO. Across the three surfaces, the estimated activated energies are 1.13, 0.94 and 1.06 eV at the Cu(1 1 1), Cu(1 0 0) and Cu (2 1 1) sites, respectively. Since the COOH-pathway involves much higher (i.e., >0.5 eV) energy than the HCOO pathway, Cu-catalyst will preferentially attack the O–H bond in FA to form the formate (HCOO) as intermediate product on all three surfaces of the catalyst. Also, the C–H bond scission in HCOO also involves a rotated molecule where the C–H bond points to the surface. At the transition state, one Cu–O bond appears broken with the C–H bond isolation occurring at the topside of a bridge at the Cu(1 1 1) and Cu(1 0 0) sites, as well as the bridge-site on the Cu(2 1 1) step, thus giving equivalent reaction energies of 0.15, 0.52 and 0.60 eV at the Cu(1 1 1), Cu(1 0 0) and Cu(2 1 1) sites, respectively; these are all indicative of the endothermic nature of the reaction on the surfaces. Both reaction and activation energies increase in the order of Cu(1 1 1) < Cu(1 0 0) < Cu(2 1 1), which are suggestive of the structure sensitivity of the reaction at the three Cu surfaces. There is a constant change of 0.26 eV in the activation energy of HCOO decomposition at all sites giving increased values of 0.95 eV to 1.21 eV to 1.47 eV for the Cu (1 1 1), Cu(1 0 0) and Cu(2 1 1) surfaces respectively, because of the strong attachment of HCOO to free open facets. These results agree with the variation in the structure-sensitive character of HCOO dehydrogenation, which is responsible for its varying activation energies at the Cu (1 1 1) and Cu(1 1 0) surfaces [66] where the measured activation energy by Nakona et al. [66] is 108 kJ/mol or 1.12 eV greater than the measured value (0.95 eV) as obtained by Li et al. [50]. Since, the activation energy of the COOH pathway is higher than that of the HCOO formation-step, it therefore suggests that the formate formation step is the rate limiting step.

Surface potential energies at the copper sites

The thermochemical properties and activation energies of the different reaction pathways were used to obtain the potential energy of the three Cu facets; see Fig. 12 a-d. The PESs shown in Fig. 12a–c can be used to compare both the HCOO and COOH-mediated pathways for all three Cu facets. However, it is evident that the PE at the HCOO-mediated pathway is more favourable than that of the COOH-mediated pathway for the FA-decomposition at Cu(1 1 1), Cu(1 0 0) and Cu(2 1 1), owing to the lower TS (transmission state) energies along the HCOO-mediated path. In Fig. 12(d) the most favourable HCOO-mediated path was examined along the three Cu facets, and it was observed that higher TS and activation energies were obtained for the HCOO decomposition step than that obtained for the HCOO formation step along the HCOO-mediated pathway. The estimated surface PEs are in the order of Cu (1 1 1) > Cu(1 0 0) > Cu(2 1 1). Thus, Cu(2 1 1) binds intermediates more strongly than Cu(1 0 0), and gives lower energies of adsorption with higher corresponding activation energies than those of Cu(1 0 0) and Cu (1 1 1). Since FA-decomposition on Cu(2 1 1) surface has a similar transition state (TS) energy with Cu(1 0 0), but lower in terms of comparing their activation energies, hence, the Cu(2 1 1) surface is therefore considered less active than Cu(1 0 0) for HCOOH-decomposition. From the PES profile, co-adsorbed formate and hydrogen (i.e. HCOO and H) depict a very stable stage, therefore, these surfaces i.e. the Cu(1 0 0) and Cu(2 1 1) surfaces, are most likely to be partly covered by the attached HCOO at the surfaces of Cu(1 0 0) and Cu(2 1 1); the last two sites bind HCOO more strongly than Cu(1 1 1) with binding energies in the tune of 0.38 and 0.60 eV, respectively. In addition, FA decomposition may prevail at the terraces of Cu catalyst, while the under-coordinated step and defect sites may become inaccessible as a result of strongly adsorbed formate (HCOO) intermediate.

Therefore, for application of an efficient catalyst system with optimum performance in ICEs, the proposed reactor-chamber for FA decomposition in automobiles can have charging pots for any of the catalysts indicated in “red colour” in refs. [38,81,87,88,108,134–136] (Table 5) and ref. [24] (Table 6). The listed catalysts that can give higher ToFs are as indicated for the references listed/highlighted in red colour in Tables 5 and 6, hence, they are all recommended for use but in terms of cost, the CuNP-tertiary amine system should be given preference, because, even the cobalt and platinum reaction systems that gave higher ToFs can only be initiated at higher temperatures say, 250 °C which gives 523 K i.e. 190 K more than the temperature required for initiating the FA-CuNP tertiary amine reaction. The intended car engine can serve the purpose of heating the reaction mixture when it runs on gasoline. Since the maximum temperature for utmost catalyst performance as indicated in this review is 90 °C/363 K, it then implies that this is achievable. The heat generated by the engine can be transferred to the reactor which must be positioned somewhat close to the engine in order to abate temperature loses. A connector system/pipe network can then help transport the gas to the hydrogen storage tank. The configuring/construction of a basal section through which catalysts/residues from the reaction can be collected for catalyst regeneration is also necessary.

Fig. 13 is the proposed reaction configuration for the automobile engine where the reaction of the amine, copper and FA is stimulated by the engine which supplies the required heat at 80–100 °C. The produced hydrogen which is collected by upward displacement of water is about 82% pure owing to the presence of CO_2. This mixture is then collected over lime water to dissolve the residual CO_2 so that the hydrogen gas becomes pure as it is stripped of CO_2. Furthermore, the gas is sent to the tank for storage and is delivered through another line that supplies fuel to the engine for mobility.

Storage and dilivery systems for hydrogen from formic acid

Despite propositions to store hydrogen in its carriers such as formic acid, there have been several concerns owing to the fact that the decomposition reaction of HCOOH for product/hydrogen-recovery will only be initiated on intermittent basis; this will not only amount to time consumption but also mar the possibility of the existence of hydrogen fuelled cars. Also, it then means that, research advancements may then necessitate the need to create reaction chambers for formic acid decomposition for hydrogen production upon the occurrence/indication of low fuel levels in cars. Also, the notion it gives strongly advocates for the purchase of formic acids at filling stations rather than H_2. Again, there may be need to constitute fuel/gas stations with plants/reactor systems for FA decomposition at such places. Since hydrogen is lighter than helium which is usually stored in weather balloons, it is therefore recommended that hydrogen from formic acid is cased in already calibrated high pressure balloons (as discussed in Sanni et al. [24] prior gas analysis), or tubes that are housed in fuel tanks with protruding hoses through the tank inlet for refuelling. It is therefore believed that this will serve as a special-housing-unit for the gas. In addition, cars with dual fuel systems i.e. with partitioned engines that can work like a partitioned

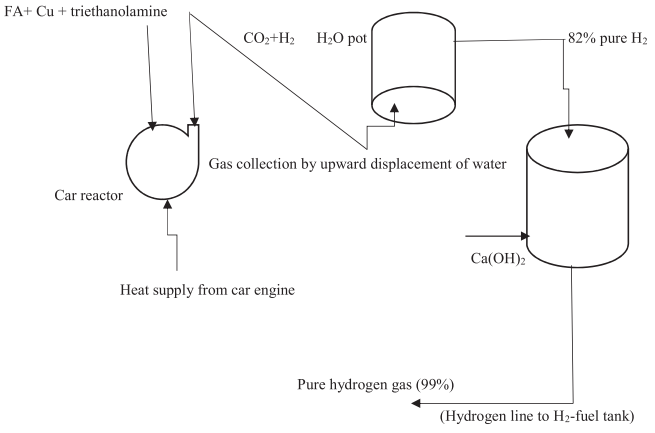

Fig. 13. Proposed reactor configuration for automobile engine.

desktop can be adopted as a way of integrating/hybridizing a dual purpose engine that can serve this purpose, such that, when a car runs short of gasoline, the car automatically activates the hydrogen fuel system to aid mobility. In lieu of the points raised, the cost of FA is also a major contributor to the marketability of this proposed system Fig. 14a-c gives an overview of the plant layout, hydrogen bank and hydrogen dispenser respectively.

Features:

Area = 4,000 m^2
Hydrogen filling capacity: 100–500 kg
Hydrogen Compressor/pump specification: booster pump / diaphragm compressor
Compressor rated working pressure: 45–87.5 Mpa
Hydrogen Storage pressure: 45–87.5Mpa
Hydrogen filling-rated working pressure 35 Mpa/70 Mpa
Hydrogen flow rate: 0.5–3 kg/min
Hydrogen Supply Method: external hydrogen supply (hydrogen bank)/FA decomposition reaction

The external hydrogen supply unit/station comprises of a hydrogen tank for unloading hydrogen from a long tube trailer. Also domiciled in the station, is a hydrogen diaphragm compressor, a storage/bank and a filling machine. The hydrogen from the tube is first compressed into at high pressure hydrogen storage cylinder by means of the compressor via the unload-line. As soon as unloading is complete, the long tube trailer can then be withdrawn from the station. After the hydrogen is stored in the hydrogen bank, the received hydrogen is then transported via a high, medium and low three-stage filling-cylinder-trail alongside the lone pipe trailer which directs the hydrogen required to fuel a typical H_2-fuelled vehicle. The merits of this design include high efficiency and early filling time; there is an assurance of good safety and reliability. Also, it is projected that 10 fuel cell buses of 8 × 140 L hydrogen tank can be filled/fuelled with hydrogen in ≤ 20 min. Based on the requirements of the process design and controls, a central control system for data generation/acquisition alongside a system monitor/Supervisory Computer Aided Data Acquisition (SCADA) system will be used in monitoring hydrogen generation and supply.

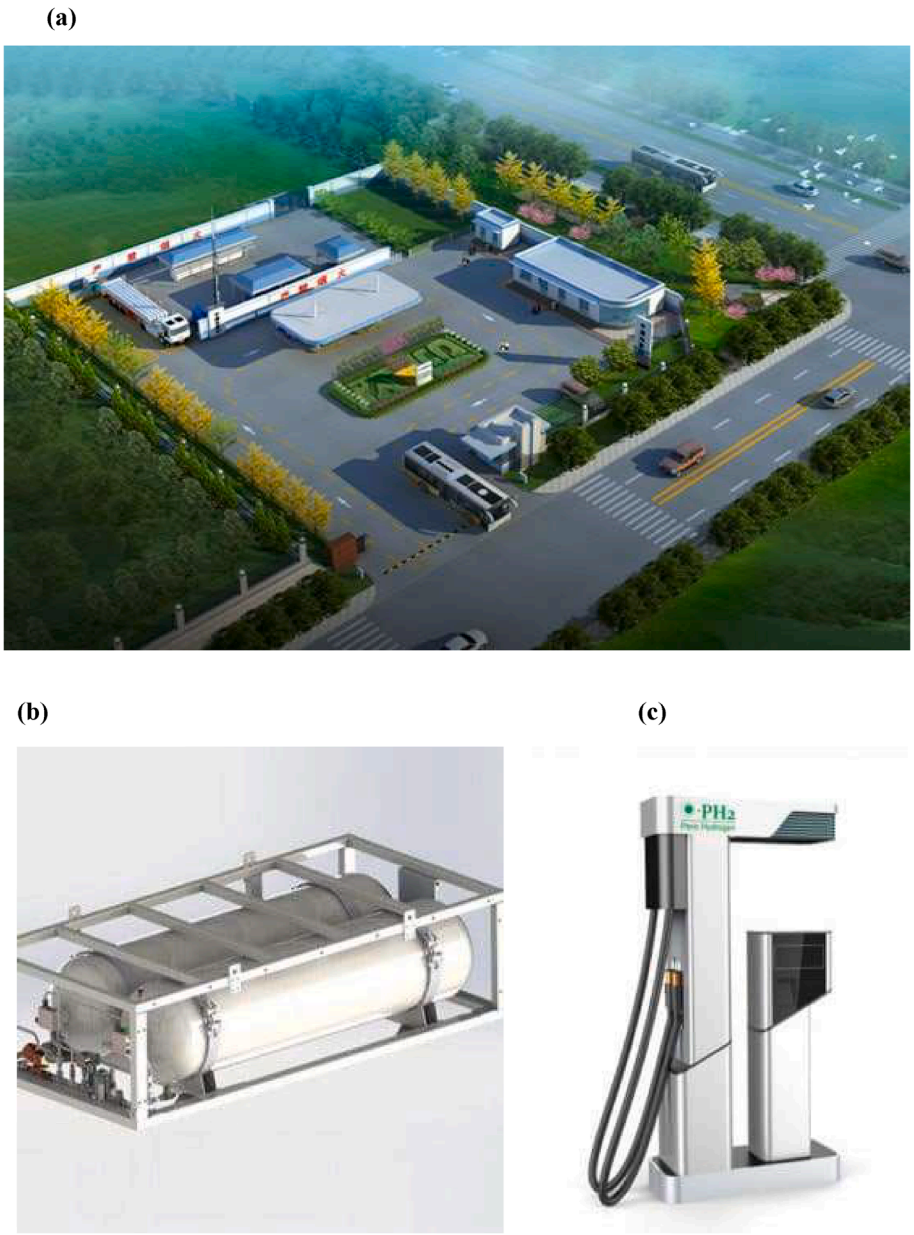

Fig. 14. a. A typical hydrogen fuel station; b. Hydrogen tanks/bank; c. Hydrogen dispenser. Adopted from webmaster@peric.com.

Life cycle assessment of the dehydrogenation process

Materials and equipment

The chemicals used for the preparation of the copper catalysts used in carrying out the dehydrogenation of FA include 99% pure $CuSO_4{\cdot}5H_2O$ salt (Fisher Chemicals), 99–100.5% Ascorbic acid ($C_6H_8O_6$) (LOBAChemie), 99% Polyvinylpyrrolidone (PVP) $(C_6H_8NO)_n$ (J.T Baker), 89.5% Formic acid (Fisher Chemicals), Triethanolamine of 85% purity ($C_6H_{15}NO_3$) (Jinhuada Chemicals), Deionized water. The equipment/apparatus used include Weighing balance, Magnetic hot plate, Measuring cylinder, Hanna pH 211 m, Gas analyser, Spatula, Beaker (1000 mL, J-Sil Borosilicate), Separating funnel (J-Sil Borosilicate, India), 3-neck round-bottom flask (J-Sil Borosilicate, India), Thermometer (0–360, Brannan, UK), Hoses, L-connector and T-connector, Magnetic hot plate, Measuring cylinder (J-Sil Borosilicate, India) and Retort stand (8 × 5 Inch, Standard Steel, India); details can be found in Sanni et al. [24]. The chemicals and equipment were handled based on the manufacturers' instructions.

CuNP-Catalyst synthesis

Environmentally friendly Cu-nanoparticles (CuNPs) were synthesized via the chemical reduction method as given in ref. [24]. 12.2 g of PVP was mixed with 1000 mL deionized water. The mixture was heated and stirred thoroughly at 60 °C. The mixture was split into two portions of 600 mL and 400 mL in separate flasks. To the 600 mL solution, 90 g of $CuSO_4{\cdot}5H_2O$ was added while 25.4 g of ascorbic acid was added to the 400 mL solution and heated at 60 °C. Upon complete mixing, both solutions, were combined, heated and stirred for 2 h at 60 °C; thereafter, the mixture was kept for 3 days to allow for efficient cooling and settling/crystallization of the nanoparticles. The supernatant solution and precipitates (0.6 M CuNps) were separated via filtration. The recovered CuNPs were washed with ethanol in order to remove excess PVP that may be bound to the CuNPs. The above procedure was repeated by preparing three separate solutions which were heated at 60 °C to give 12.2 g of PVP in 1000 mL of deionized water. 4 PVP solutions were prepared, each of 500 mL volume. In two of the 4 PVP solutions, 75 and 90 g of $CuSO_4{\cdot}5H_2O$ salts were added, while 59.8 and 70.4 g ascorbic acid were added separately to the other two PVP solutions respectively, which gave corresponding molarities of 0.8 and 1 M CuNPs. To another PVP solution, 120 g of $CuSO_4{\cdot}5H_2O$ was dissolved in 12.2 g/1000 mL PVP solution, 70.4 g ascorbic acid was added and the mixture was heated to 60 °C. The CuNPs of 0.8–1.2 CuNPs were then recovered as already discussed for the case of 0.6 M CuNps. The pHs of the solutions were measured.

The reaction system

Fig. 15 is an illustration of the simulated glass reactor and gas collection set-up. Control experiment: 10 mL FA was measured and transferred into a three-neck flask and heated to 80 °C using a magnetic hot plate; the volume of hydrogen evolved was recorded. 25 mL triethanolamine was added to 10 mL FA in a flask. The mixture temperature was raised to 80 °C. Four mixtures, each containing 25 mL triethanol amine and 10 mL FA were prepared. 1.0 g each of the 0.6, 0.8, 1.0 and 1.2 M CuNP was measured and added separately to 4 mixtures and heated to 80 °C. The volume of gas evolved was measured using water displacement method. The reaction was very slow for FA-amine system without catalyst compared the reaction aided by the CuNPs. To justify the reusability of the best catalyst (1 M CuNPs) as established from the reaction, 1 g of the 1 M CuNPs was collected for reuse after 6 h of hydrogen production. The produced hydrogen was measured and contained in a balloon after each run. The system was allowed to cool to 25 °C, after which it was recharged with 10 mL FA for the next operation vis-à-vis the 23rd run.

Note: It is necessary to add the amine prior the nanoparticles rather than the reverse because, the latter will not give any visible reaction. Also, the CO_2 release was about 9.5% with 82.7% volume of hydrogen recovered. A total of twelve components were identified by the gas analysers. Also, the automobile reactor will simulate the glass set-up and its material of construction is stainless steel, which is durable, sustainable and corrosion resistant. However, in situations of minimal corrosion which may exist in form of oxygen corrosion- caused by the contact with O_2, sweet corrosion- caused by CO_2, sour corrosion- caused by H_2S, crevice corrosion- which occurs by stagnation of fluid in narrow clearances, microbial corrosion- which is caused by the metabolic activities of microbes, fretting corrosion- caused by friction on metallic parts, galvanic corrosion- caused by the difference in the nature of metals that make up an alloy such as steel, erosion corrosion- caused by the removal of an initial deposition of a protective corrosion product/impervious layer that serves as protection for a metal, leaching- the destruction/reduction in the properties of one metal relative to another in an alloy, stress-induced corrosion- caused by the continuous application of stress on a metal surface, fatigue corrosion- caused by failure of a metal due to fatigue which is caused by cyclic concentration of stress on a localized area, flow-induced corrosion caused by the flow of a fluid onto/over a metal surface, in the presence of an electrolyte, all of which can be controlled via any of the following methods when applied under the most suitable conditions.

Cathodic protection: This is of two forms (impressed current and sacrificial anode-protection); for impressed current mode of protection, a direct current is applied in the reverse direction of the flow of current through the affected metal surface since corrosion is influenced by the setting up of an electrochemical cell within the metal. For the sacrificial

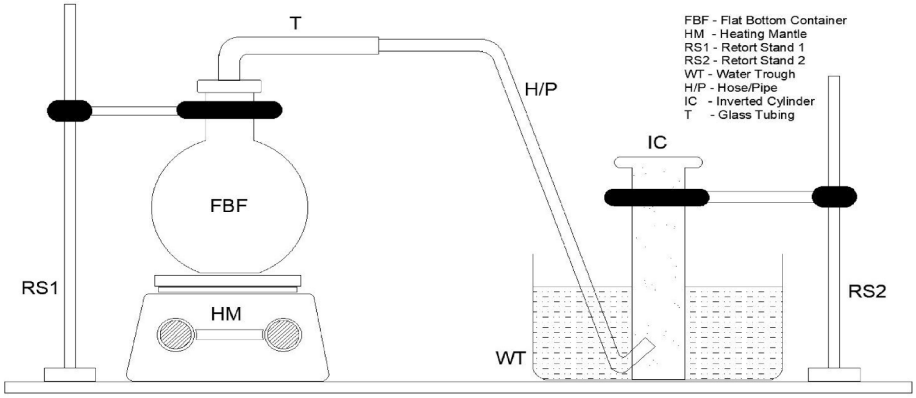

Fig. 15. Experimental setup for the dehydrogenation of formic acid. Adapted from ref. [24].

anode mode of protection, a metal higher up in the galvanic series than the supposed donor-metal in an alloy, is coated with the metal of higher activity; the essence is to sacrifice it for the actual anode, hence, the sacrificed metal is termed the sacrificial anode [137]. James and Bushman [138] discussed pipe/metallic corrosion and inhibition in relation to the use of impressed current or sacrificial anode methods of corrosion protection.

Coating and painting: This method involves the use of coloured pigments such as corrosion resistant liquid-pigments or paints and coats that have high binding strengths with the metal to be protected [139]. Although, in some instances, however good a coat is or however well applied, it may peel off over time owing to mesa attack or cathodic disbondment, hence the need to carefully select very effective choice pigments/coats as corrosion inhibitors Sanni et al. [140].

Curable coatings at temperatures less than 80 °C with low hydrothermal stabilities are required for preventing the corrosion of HX heat exchanger tubes and pipe joints after roller expansion or welding. However, for higher temperature applications, these equipment need to be coated with materials that can withstand temperatures > 200 °C, have good adherence to the metal surfaces and possess the ability to become cured at temperatures up to 80 °C and can be applied with a paint, brush or spray gun. Poly(tetrafluoroethylene)/(hexafluoropropylene) (PTFHFP) polymer coatings have been tested as corrosion mitigators for carbon steel joints in brine heated up to 200 °C. However, the efficacy of the inhibitor was found to gradually wane after 20 days of application at such temperatures, thus suggesting that they may perform better at lower temperatures since thermal oxidation sets in after the 20th day [141], hence, there is need to modify this inhibitor for application within longer periods at high temperatures using high temperature resistant materials such as multiwalled carbon nanotubes (MWCNTs), zeolites, metal organic frameworks etc. for improved performance.

The pulsed magnetic sputtering method (PMS) is an approach used to deposit/coat a wide range of materials for the enhancement of film properties and flexibility in low friction titanium nitride coats and aluminium doped zinc oxide conductive transparent oxide sputtered directly from powder targets of thin film photovoltaic devices comprising of copper (indium/gallium) diselenide; sputtering is usually done at radiation frequencies of 20 – 350 kHz [142].

Chemical inhibition/injection: This involves the use of chemicals (organic or inorganic) such as glutaraldehyde, sodium tungstate, etc. in single or combined forms such as sodium nitrite, zinc nitrite and sodium tungstate [140] as means of protecting metal surfaces against corrosion. Ngobiri et al. [143] compared the performance of *Sulfadoxine–Pyrimethamine* (SP) as a corrosion inhibitor for petroleum steel pipe. The work of Li et al. [144] confirms the protective ability of D-phenylalanine as a corrosion inhibitor for Q235 carbon steel.

Continuous monitoring and inspection: Till date, this remains one of the most effective approaches of guiding against any form of corrosion since, it involves constant survey and observation/visual inspection of the metal while carefully checking for the appearance of corrosion spots/scales in order that apt measures are taken to abate the degradation of the metal [138]. Hector and Liz [145] extensively reviewed biocorrosion and biofouling of industrial equipment in which real time environmental monitoring and inspection were adopted as a means of mitigating metal decay.

The use of plant extracts: This is one of the most current environmental technologies adopted till date. It involves the use of extracts of plants such as Fenugreek seed oils and bitter leaf oils [146], modified-tannin solutions, plant DNA (Calf thymus gland-DNA) [147] etc. as corrosion inhibitors. The inhibiting behaviour of leave and seed extracts of Phyllantus amarus on mild steel corrosion in aqueous HCl and H_2SO_4 have been studied using weight loss and gasometric methods [148]. Henna (*Lawsonia inermsis*) extract and its constituents (lawsomne, gallic acid, α-D-glucose and tannin acid) were also confirmed to exhibit corrosion protection abilities for steel by Ostovari et al. [149].

Additive manufacturing and laser/light cladding: This method involves the integration of corrosion resistant metals (Cu, Ni, Cr, etc.) or alloys such as TiC in other metals/alloys as a means of improving the metal's composition all aimed at taking advantage of the synergistic effects offered by the blended metals; with the help of high laser concentration of beams some of these metals with high melting points can be brought to their molten states for easy/efficient mixing with other metals. In laser cladding, one metal i.e., the more corrosion resistant metal clothes or wraps the other in order to improve the service life of the less corrosion resistant metal. This approach helps to moderate the costs involved in using an expensive metal in entirety in combatting corrosion; for instance, the cladding of TiC and TiN on tungsten carbide [150]. The method employed involves the physical vapor deposition (PVD) by cathodic arc using a system bias and Cathodic arc evaporation techniques.

AM technologies are in two categories namely (a) powder bed fusion (PBF) which includes selective laser melting (SLM) or electron beam melting (EBM) and (b) direct laser deposition (DLD) or direct energy deposition (DED), which entails the simultaneous surface-supply of the material and energy needed to build the desired surface. Other AM methods include welding and cold spraying [151]. Additive manufacturing (AM)/3D printing is currently one of the mainstream approaches for producing metallic components from alloys owing to the different advantages which the process offers, which include net shape, material management, adaptability to low volume of production runs, and the flexibility towards exploring alloy compositions which were not accessible to conventional casting methods. AM entails the use of laser/electron-based local melting which plays a significant role in ensuring a well-blended alloy microstructure. In the review conducted by Sander et al. [151], the corrosion of alloys made by AM/laser/electron-based methods were considered, where they considered several works that bother on metallic corrosion in relation to AM; the relationship between corrosion resistance of AM-manufactured metals and their unique features such as porosity, grain structures, dislocation networks, residual stress, solute segregation, and surface roughness were discussed and they affirmed that, AM-manufactured metals were found to be more corrosion resistant than those manufactured by conventional casting methods.

Gas collection approach and volumetric estimation of H_2 gas

The gas produced from the reaction of 1 M CuNPs and the formic acid-triethanolamine mixture already discussed, was determined by water displacement of the gas. The setup adopted includes an inverted graduated cylinder which was placed over a trough filled with water. At the expulsion of gas from the reaction flask, the light gas meandered through the water in the trough by diffusion and found its way to the top of the cylinder since it is lighter than water; this helped to balance the pressure within and outside the cylinder. Using the ideal gas and Dalton's laws, the partial pressure of hydrogen gas collected over water and the total pressure of the system were determined (see Sanni et al. [24] for details).

Hint: The pressure of the released gases, are indicative of the relative pressure of hydrogen compared to other gases. Based on the estimated pressures, the partial pressure of the gas is not high enough to engender unsafe conditions, however, since, hydrogen gas is highly flammable, four options may suffice for the gas containment in tubes, banks/cylinders or balloons made from polyester and coated with polyurethane.

i. Hydrogen can be stored in high-pressure resistant cylinders

ii. The produced hydrogen can be stored in special balloons constructed with pressure resistant/high texture-polymers and lined with non-porous membranes to avoid leaks in the event of any piercing of its external part by any object. However, for safety, the balloons can be enveloped in an inert atmosphere blanketed with N_2 or solid CO_2 to avoid eventualities, in case of tendencies for fire hazards caused by other operations within the plant. Better still, owing to the fact that, the

scientific world still finds it difficult to accept the sustainability of balloons for hydrogen storage, hydrogen tubes/banks made of stainless steel, can be adopted for storing the produced hydrogen.

iii. The produced hydrogen can be liquified at − 252.87 °C in order to increase its energy density prior storage; till date, this appears to be the most appealing and promising alternative for storing hydrogen, however, the process is energy intensive and will add to the overall cost of producing hydrogen, hence, options ii and iii require considerations with good safety practices for efficient implementation.

Gas analysis

The composition of other gases released are as given in Table 7 with the measured proportions of the CH_4, O_2, CO, H_2, CO_2, NO_2, NO, SO_2, HCOOH, H_2S, CO_3, NO_3 taken from the gas analyser being 12%, 4%, 12 ppm, 82.2%, 9.5%, 6 ppm, 24 ppm, 1 ppm, 0.01%, 0.01 ppm, 13 ppm and 19 ppm respectively. This clearly reveals the quantities of emissions associated with the product (hydrogen). Furthermore, almost all the FA was used up, such that only 0.01% of FA was left unconverted. The low compositions of the other gases such as CO, CO_2, NO, NO_2, SO_2 and H_2S resulting from the dehydrogenation process, are also evidences of the impact of the resulting emissions associated with this process. There are also supporting evidences that hydrogen burns as a clean fuel. Furthermore, the alkaline system for trapping CO_2, is so that there is little or no release of CO_2; there is also the likelihood of CO being trapped by the alkaline solution shown in the process flow scheme of the designed reactor.

Kinetics of the FA-Dehydrogenation: Volume-conversions for FA-dehydrogenation and gas emissions

The plausible mechanism for the reaction between FA-amine mix and CuNPs is given below:

$$HCOOH \overset{R1R2-NH2/Cu2+}{\rightarrow} CO_2 + H_2 \quad (14)$$

The kinetics of FA-decomposition is somewhat complex because, for one to be able to properly study the process kinetics, the system's species-concentrations need be monitored as reactants and products disappear and evolve respectively. This is somewhat herculean since the reaction ought to be interrupted at different times so as to be able to adequately estimate the amount of FA spent or left while the reaction is in progress. Striving to monitor the rate of formation of hydrogen while the reaction is in progress will cause some of the produced hydrogen to be lost, hence, the need to adopt the DMA with a few basic assumptions (i.e. major products being CO_2 and H_2) which helps to overcome that challenge; stoichiometric quantities of hydrogen can then be expressed in terms of the formed products CO_2 and H_2 only, as given in the mechanism for dehydrogenation. This then implies that going by the process kinetics, other constituents such as CH_4, NO_3, CO etc. were assumed to be present in insignificant quantities, otherwise, the kinetic scheme established by Sanni et al. [24] would involve complex species which makes it very difficult to resolve; however, the kinetic scheme showed appreciable levels of accuracy of about 82.7%.

Here, a back-calculation approach was used in investigating the kinetics of FA-dehydrogenation. It was assumed that the reaction reached completion in 6 h and that the highest volume of recovered hydrogen was 815 mL since no gas was evolved at further times, hence, the volume of gas produced was taken to be the maximum recoverable value (i.e. 100% H_2 in FA = 4.3 wt% = 815 mL). The reactants and products were also assumed to exist in liquid phase all through the reaction time, thus implying that the system was homogeneous and the reactor was described as a variable volume batch reactor whose expansion factor was estimated to be 1 i.e. $\varepsilon_a = 1$. Since no free-hydrogen was initially present in FA and the reaction is deemed irreversible at the stated conditions, the volume produced/max volume = approximate conversion of FA to hydrogen.

Comparing the results from the process kinetics with the results obtained from the gas analyser, the process scheme guarantees about 82.7% accuracy with an estimated inefficiency of 17.8%, hence, the kinetic data is dependable and reliable. Although, improvements are required considering the need to involve other species in the Differential Method of Analysis (DMA) calculations i.e. since CO_2 and H_2 make up about 91.7% of the total gas released, 8.2% of the constituents need to be factored into the process kinetics. In addition, the 1st order description of the dehydrogenation process, assumes that all the FA is used up with zero/negligible amount of CO_2, whereas, based on the data obtained from the gas analyzer, only 82% H_2 was formed. Furthermore, the formation of NO_X gases may be due to the reaction between nitrogen in the triethanolamine and oxygen in FA. Other constituents such as sulphur and hydrogen sulphide, found in the gas, may have been introduced by the CuNP-catalyst which had some sulphur imposed on it by its precursor during synthesis and the combination of H_2 from FA and sulphur in the CuNPs, respectively. It is also important to note that the reactor size should be about 110 mL to provide for clearance and reduce the pressure of hydrogen which somewhat raises its energy density and limits the tendency for emergencies.

Table 7
Percentage composition of gas in H_2 sample.

Component	Chemical formula	Composition (%, ppm)
Methane	CH_4	12%
Oxygen	O_2	4%
Carbon monoxide	CO	12 ppm
Hydrogen	H_2	82.2%
Carbon dioxide	CO_2	9.5%
Nitrogen dioxide	NO_2	6 ppm
Other (Nitrogen oxide gas derivatives)	NO_X	24 ppm
Sulphur dioxide	SO_2	1 ppm
Hydrocarbon (Unused HCOOH)	HCOOH	0.01%
Hydrogen sulphide	H_2S	0.01 ppm
Trioxo carbonate VI gas	CO_3	13 ppm
Trioxonitrate V gas	NO_3	19 ppm

Source: Sanni et al. [24].

Pros and cons of the 1 M CuNP-catalyst for FA-dehydrogenation

Pros

- The 1 M CuNPs had an induction period of 10 mins which is quite impressive.
- 815 mL of H_2 was collected after 6 h of reaction time.
- The process of synthesizing the catalyst is not herculean and its precursor ($CuSO_4.5H_20$) is readily available/affordable
- Problems such as the influence of steric hindrance begin to arise after 20 cycles of hydrogen production within 120 h with an established reusability of 1 g CuNP catalyst for every 2000 mL FA.
- A low catalyst-amine ratio is required for the dehydrogenation process.
- There is a high theoretical conversion of 100% with a corresponding actual conversion of 82%, in 6 h; comparing this with the results in Table 8, shows that the degree of conversion for other heterogeneous catalysts are quite lower relative to that estimated for the CuNp catalyst-system, thus confirming a better performance of the CuNP-catalyst.
- The CuNPs + FA-amine reaction system gave a boost in hydrogen production by 11.3 times the uncatalyzed reaction (i.e. the FA + amine system, whose volume of produced H_2 = 72 mL in 6 h), whereas, it was about 13.81 times the volume of H_2 (59 mL) obtained for the reaction involving only FA without the amine and CuNPs.

Table 8
Efficiencies of catalysts for FA-dehydrogenation reactions.

Catalyst	T (K)	ToF initial (h^{-1})	Eff.Conv.(%)	Ea kJ mol-1	Ref.
$Pd_{60}Au_{40}/Z_rSBA$-15-AP	298	1185	95	42.5	[123]
Pd/CNx	298	639	98	48.8	[124]
Ag@Pd/C	298	157	43	–	[152]
AgPd/C	298	274	46	22.0	[125]
AuPd/C	298	41	24	28.0	[86]
CoAuPd/C	298	54	91	–	[84]
NiAuPd/C	298	20	73	–	[126]
AgAuPd/rGO	298	95	100	–	[127]
CoAuPd/r-GO	298	63	51	–	[153]
CoAuPd/DNA-rGO	298	130	96	–	[153]
AuPd/N-mrGO	298	39	93	–	[83]
Au@Pd/N-mrGO	298	111	98	–	[83]
AuPd/N-rGO	298	17	57	–	[129]
AuPd-CeO2/N-rGO	298	68	98	–	[129]
AuPd/ZIF-8-rGO	298	532	83	–	[99]
CuNPs	353	135.8 mL/h (5.98)	82 (actual)	–	[24]
			100% theoretical		

*ToF = Turn over Frequency, Eff.Conv. = Efficiency of conversion, Ea = Activation Energy.
Adopted from ref. [24].

- Higher conversions were attained for the Cu-tertiary amine system than many heterogeneous catalysts which are composites of very rare and scarce metal-precursors that make the FA-dehydrogenation more expensive (see Table 8 for some listed heterogeneous catalysts for FA-dehydration).
- The dehydrogenation kinetics is reliably accurate considering the accuracy of the estimated volume of the synthesized hydrogen, as well as the kinetic parameters (reaction-order, rate constant, conversion, partial pressure etc.), which gave a clear insight on the influence of pH, catalyst concentration, time and catalyst size on the dehydrogenation process.

Cons

- The 1 M CUNP-catalyst used is restricted to activation temperatures $\geq 80\,^{\circ}C$.
- The catalyst loses its reactivity after 20 cycles hence, catalyst regeneration/refilling is required after the 20^{th} cycle [24].
- The energy requirement for reaction initiation of the CuNP + FA-amine system is higher relative to those of some available heterogeneous catalysts, i.e., the reaction described for the CuNP + FA-amine system requires higher energy input. However, this should not pose any problem as the heat required to initiate the reaction will be harvested from an automobile engine.
- The process kinetics discussed here, will need some form of modification if it must be adopted for situations involving heterogenoeus catalysts.

The results in Table 8 show that the 1 M CuNP-catalyst gave higher conversion than the catalysts adopted in refs. [86,125,126,129,152,153]. Although, a lower turnover rate of H_2–production i.e. ToF of 5.98 $h^{-1}$was recorded for the CuNP-tertiary amine system, the new Cu-tertiary amine system gave higher conversion relative to some of the multitudinous/heterocatalysts presented in Table 8. No doubt, these hybrid catalysts, will increase the overhead cost incurred in producing the catalysts. Comparing some homogeneous catalysts as presented in Table 9, it is somewhat obvious that the recorded ToFs are lower than that obtained for the CuNP-tertiary-amine system because, the recorded ToFs are measures of the average

Table 9
Number of Active sites (Ns), Steady-state activity and ToFs of other homogeneous catalysts at 250 °C compared to the Cu-tertiary amine system.

Catalyst Ns a (μmol/g)	Number of active sites (Ns)	HCOOH Activity 250 °Cb(μmol/g•s)	TOF 250 °C s^{-1}
Co	$3.1*10^{1}$	$9.3*10^{-2}$	$3.0*10^{3}$
Fe	$1.8*10^{2}$	$4.0*10^{0}$	$2.2*10^{-2}$
Ag	$7.6*10^{0}$	$3.0*10^{0}$	$3.9*10^{-1}$
Au	$5.2*10^{1}$	$4.0*10^{1}$	$7.7*10^{-1}$
Ni	$1.6*10^{2}$	$1.5*10^{3}$	$9.3*10^{0}$
Rh	$1.5*10^{1}$	$4.8*10^{1}$	$3.3*10^{0}$
Pd	$9.9*10^{1}$	$1.6*10^{2}$	$1.6*10^{1}$
Cu	$1.6*10^{1}$	$5.2*10^{1}$	$3.2*10^{1}$
Pt	$1.9*10^{1}$	$1.8*10^{3}$	$9.8*10^{2}$
CuNP-amine	$4.35*10^{0}$	ND	$358.8*10^{0}$ @ 80 °C (this work)

Source: Sanni et al. [24].

hydrogen production rate for each catalyst. Thus, it is apt to infer/conclude that the Cu-amine system outperforms all the homogeneous catalysts presented in Table 9 owing to its higher ToF value of 358 s^{-1} as well as the volume of hydrogen produced from the reaction-system.

The durability of the CuNP-catalyst was determined by carrying out several runs of the FA-conversion using the 1 M CuNPs. It was observed that the catalysts retained their colour and catalytic activity in the reactor up until the 20^{th} run/cycle (see details in ref. [24]), beyond which the CuNPs began to appear slightly oxidized/decolourized; they assumed a greyish black colour which is the colour of copper I oxide. This may have been caused by the influx of oxygen into the reactor upon recharging/replenishing the flat-bottom flask with fresh FA. Also, beyond the 20^{th} cycle, catalyst poisoning by CO may become prominent, thus reducing the number of surface-active sites on the CuNP-surface. Upon adding more FA, it was observed that, the resultant rise in the volume of hydrogen produced may have resulted from the erosion of any deposited inhibitor on the active sites of the CuNPs, thus ensuring higher reactivity, hence the reason for the slight undulating rise in H_2 production despite the drop in H_2 production at some point where the system began experiencing appreciable drop in the volume of synthetic hydrogen over previous runs. The stability of the CuNPs in the reactor would have been altered by the uncapping/removal of the capping agent which helps secure their stability.

Essentials of the CuNP + FA-Amine system

The efficiency of the reactor is a function of the degree of conversion of the FA to hydrogen gas. Four factors responsible for the degree of conversion of FA to hydrogen include pH of catalyst-solution, concentration of the CuNPs catalyst, reaction time as well as the size of the catalyst.

Particle-screening tests for the best CuNP-concentration for FA-dehydrogenation

Even when the same quantity of catalyst i.e. 1 g of catalyst was used for the entire process, changes in the CuNP-concentration from 0.6 to 1.0 M increased the theoretical and actual FA-conversions from 59 to 100% and 59–82.2%, respectively after 6 h. However, at higher than 1 M concentration of the CuNP-catalyst, FA-conversion/hydrogen production dropped to 52%. This then shows that, the highest hydrogen production corresponds to CuNP-catalyst concentration of not less or>1 M; this obeys the law of mass action, which states that an increase in concentration, can speed up the rate of a chemical reaction. The observed trend justifies the results of the catalytic dehydrogenation process, especially at the optimum CuNP-concentration (i.e. 1 M concentration) as observed by Sanni et al. [24] (Table 10). Catalyst-concentration is a

Table 10
Volume of hydrogen produced for catalyzed/noncatalyzed reactions involving FA.

Catalyst	Volume per hour of Hydrogen produced (mL/h)
Akbayrak et al. [154]	
Pd/CeO_2	65
Pd/ZrO_2	10
Pd/TiO_2	10
Pd/SiO_2	12
Pd/Al_2O_3	5
Pd/HfO_2	0
Sanni et al. [24]	
FA only	10
FA + Triehanolamine	16
0.6 M CuNPs + FA + Triehanolamine	10
0.8 M CuNPs FA + Triehanolamine	80
1.0 M CuNPs FA + Triehanolamine	800
1.2 M CuNPs FA + Triehanolamine	50

Source: Sanni et al. [24].

measure of the number of moles of catalyst used per unit volume, therefore, at 1 M concentration of the catalyst, there were more FA-molecules interacting to produce the desired hydrogen, whereas, at lower catalyst-concentrations i.e. below the optimum CuNP-concentration, the relative number of active catalyst-molecules, per unit volume of solution reduces, which results in lower conversions or lower volumes of hydrogen.

The need to control catalyst-size

It is often difficult to produce nanoparticles of same size, hence, the need for an improvised approach for establishing the effect of CuNP-particle size. In ref. [24], the synthesized CuNPs were of varying sizes, however, an average particle-size was obtained for every batch-concentration of synthesized CuNP-particles. For larger particles, the surface area to volume ratio is usually lower compared to particles of smaller diameters, hence, there are more active sites in the latter relative to the former. Furthermore, considering the law of mass action, a reduction in particle/catalyst-size enhances the degree of conversion. This justifies the fact that the highest possible conversion/hydrogen production was obtained for the smallest particle size of 1.5 nm with corresponding concentration of 1 M.

Essentials of controlled solution-pH of the CuNP catalysts

The pH of a system is a measure of its alkalinity or acidity, thus, low pHs inform higher acidic strengths and vise-versa. Based on the investigation, in order to achieve > 50%, but less than 70% hydrogen production from FA, the pH of the CuNP-catalyst should span from 2.5 to 2.9. However, if a theoretical/actual conversion of 100/82% is desired, the most desirable pH of the CuNP catalyst is 3.19, this also doubles as the optimum pH. At CuNP catalyst-pH of 2.5–2.9, the actual hydrogen volume was less than 82%, thus giving a conversion > 52 but less than 82%. Comparing the results with the results of Wang et al. [7], in which a pH of 6.5 and a maximum amount of hydrogen of 2.46 mmol/L/D was obtained for a reaction time of 0–6000 mins. The difference in pH between the 1 M CuNP-system and the results obtained in ref. [7] was allotted to the difference in the nature of raw materials adopted in both research works, (FA-Cu-tertiary amine system and lignocellulosic biomass), as well as the catalyst-type (i.e. Cu and cellulose/β-glucosidase enzymes as catalysts), respectively. The latter also underwent simultaneous saccharification and fermentation steps prior to obtaining synthetic hydrogen. Based on the reported pHs of both systems, it then implies that the pH of the CuNP-solution is more acidic (3.19). Hence, in order to abate the situations of reactor material corrosion, the proposed material of construction for the reactor is stainless steel, which is highly resistant to all forms of acid corrosion. Furthermore, periodic checks/inspections would be conducted as corrosion control measures in order to ascertain whether there is any need for cathodic protection, constant inspection and monitoring, painting- with heat resistant paints, coating/electroplating, chemical injection, laser cladding etc. as ways of ensuring a longer service-life of the material of construction.

Monitoring reaction time

Reaction time is also of paramount importance in the FA-dehydrogenation process. For the CuNP-tertiary amine system, the volume of hydrogen produced, increased with reaction time. At 0–10 mins, the CuNPs began to have effect on the volume of H_2 released from the FA. Below the peak period (6 h), the volume of hydrogen produced from 0 to 360 mins increased progressively at every 60 min-interval (Table 10).

The hourly-hydrogen production rate of some catalysts used by Akbayrak et al. [154] gave lower volumes of hydrogen production when compared with those recorded of the 1 M CuNPs + Cu-amine system. This further justifies the outstanding performance of the catalyst-amine system for FA-dehydrogenation.

Cost of chemicals and reagents

Based on the estimated costs at the time of this investigation (July 2019), the cost of the 500 g copper sulphate pentahydrate salt was 7,500 naira (i.e. $ 20.83 (USD)), 500 g ascorbic acid = 7,700 naira (21.39 USD), 500 g PVP cost 29,000 naira (80.56 USD) and the cost of 500 mL of FA = 10,000 naira (27.78 USD). The then estimated total cost of reagents/chemicals was N 49,200 = 150.56 USD, which implies that the cost of all relevant chemicals = N 49, 200 (i.e. 49, 200 naira) or 150.56 USD, which suggests that the estimated cost is quite cheap and affordable compared to those of other heterogeneous catalysts which will not only increase the cost of procuring chemicals/reagents, but also add to the overall/overhead cost, thus making the process to be more expensive.

Gas balloon/buffer and tubes/cylinders for storage of H_2-gas

Gas storage systems, range from cylinders to tubes which are compact and shaped to withstand gas pressures. Gas balloons/gas holders, gas-bags and gas recovery membranes (Fig. 16a-h) are also being used, which are flexible, inflatable bladders that are suitable for industrial applications, especially in sectors such as breweries, technical universities, research institutes and special recycling systems. They often serve as conventional/economic storage systems for gases such as N_2, CO_2, H_2, He or other inert gases. For optimal and cost-effective use, these systems are gas-tight with their sizes usually spanning from 0.5-7500 m^3 (17 cubic feet to 265,000 cubic feet) and may assume geometries such as spheres, cylinders, angular or cushion, pillow and custom shapes, based on the desired spatial conditions.

Custom shapes or sizes for H_2-balloons

These flexible tanks offer the following merits: they are light in weight such that they can be inflated and deflated with ease hence, this expedites their installation or removal when the need arises. Based on customer specifications, they may be fitted with inflation and deflation adapters, such as clamps or screws on flanges constructed with stainless steel or other flexible fittings made from gas storage fabrics.

Special fabric for H_2-buffers

Gas storage balloons are made from a very robust polyester fabric,

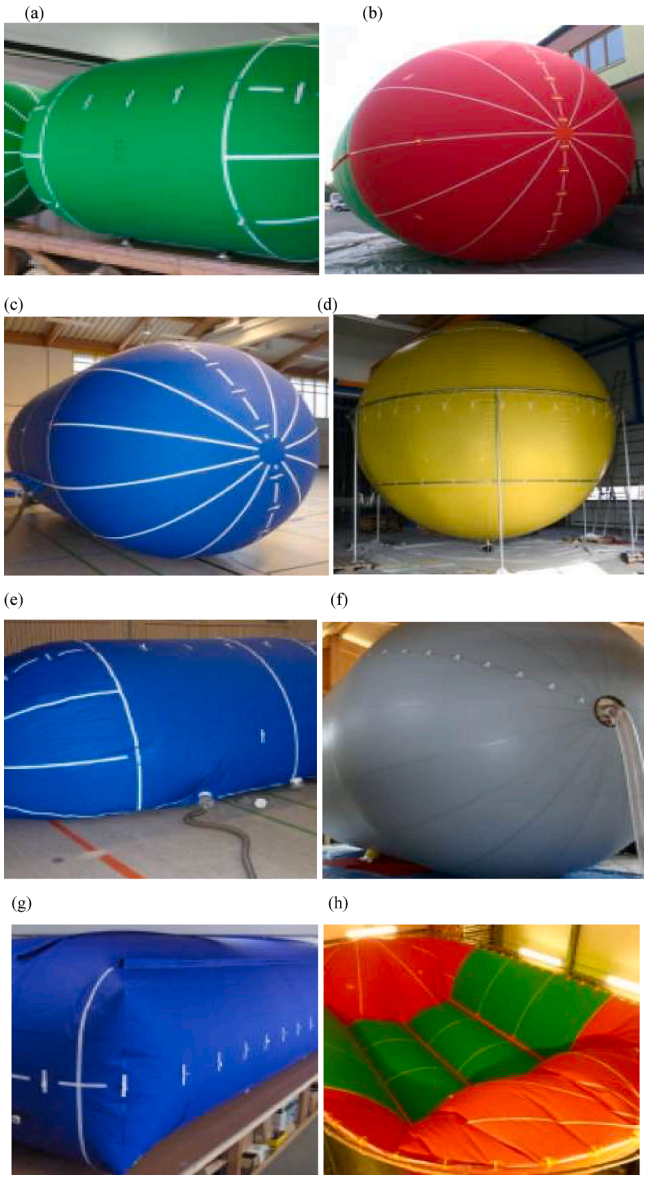

Fig. 16. a-h: Different shades of H_2-gas buffers/balloons.
Source: https://www.ballonbau.de/en/sport-balloons [155]

coated with polyurethane on both ends. The fabric is designed to have a gas diffusion rate of less than 1 L/m^2 in 24 h (i.e. 0.292 ft/h) based on its calibration with helium gas at 20 °C. To guarantee efficient/effective storage of several gases, each gas collector is designed for a specific type of gas. In other to meet the safety guidelines of the United States Department of energy (DoE), other special safety measures include, subjecting the balloon fabric to a special antistatic treatment.

Securing and anchoring H_2-Gas balloons using special tubular frames

In order to keep the hydrogen gas balloons standing securely at their installed locations, the balloons need be suspended in tubular frames which may be suspended from the top/ceiling using steel cables that are fixed to the floor with basal supports. Based on their modes of design, the procedures do not require any skilled expertise as they can be easily understood and followed aptly by a reliable technician. In order to also guide against risks, the balloon is integrated with a safety mechanism to help guide against unintended over-inflation. The hydrogen-fill level of the H_2-gas balloon is monitored using special wire-actuated encoders, as well as ultrasonic laser distance meters.

Conclusion

Indeed, there is no doubt about the possibility of hydrogen becoming the fuel of the future if all the already discussed sources are fully exploited to produce commercial quantities of FA for commercially synthesized hydrogen gas. The adoption of some very efficient catalysts with less poisoning potentials, have been proposed for FA-decomposition reactions. Also, it becomes very pertinent to mention that, the idea of producing hydrogen from FA regardless of its precursor/source is guided by the process economics, market demand, and environmental policies as regards the world's clean energy policy. Several precursors (fossil fuels, nuclear power plants and renewable sources), such as biomass, wind, solar can be used to produce FA and thus H_2; based on the description of the Energy Institute for hydrogen production processes, hydrogen recovered from natural gas with its CO_2 emissions captured is known as blue hydrogen, whereas, if the hydrogen source is natural gas and the CO_2 released is vented into the atmosphere, the hydrogen is tagged grey hydrogen, however, hydrogen produced from renewable energy/electricity with no CO_2 emission is tagged green hydrogen but hydrogen from coal with CO_2 vented into the atmosphere is labelled brown hydrogen; hence, the scheme described in this study falls into the blue hydrogen class where the associated CO_2 is trapped in an alkaline medium. Hydrogen can serve as an alternative/additional energy carrier, which will encourage further domestication and exploitation of national resources/industrial processes towards full utilization of hydrogen, thereby reducing overdependence on the importation of petroleum. ICEs/gasoline engines can be modified or preferably, new engines can be manufactured to suit the use of H_2 as fuel when these processes become fully commercialized. Without the use of catalysts, the quantity of hydrogen produced with time is highly energy consuming which will yield very high investment costs compared to the catalysed processes. Besides high-pressure cylinders, balloons can be used for the storage of hydrogen. Tubes are also proposed for the storage of hydrogen gas in cars, as well as the need to site FA conversion plants at hydrogen-fuelling/refuelling spots. In order to use hydrogen safely, leak-prevention, scenting with neutral constituents to give it an identifiable smell, flagging off hotspots with danger signposts, transporting it carefully and controlled burning of the gas, can help minimize the risks associated with storage. In addition, the gas can be stored in high-pressure cylinders, or in high-texture polyurethane balloons, which may be kept in isolation or underground, within a suitable geology such as salt caverns, so as to abate adverse consequences in cases of emergencies. In today's world, over 95% of the world's hydrogen is obtained from natural gas or coal, which usually give off greenhouse gases which trap the released heat and emits it into the earth's atmosphere, thus giving rise to high global temperatures and emissions. Sourcing for alternative fuel that is sustainable and gives less emissions underscores hydrogen as a viable alternative to fossil fuel. Therefore, switching to a low-carbon method of producing hydrogen requires that it must have little or no environmental impact, hence the need to choose apt feedstocks such as formic acid, while bearing in mind the energy required to drive the process. Based on the process scheme portrayed in this review, it is evident that, hydrogen-fuelled cars will soon be the spate of future automobiles.

Data availability

All data for this manuscript are already included in the manuscript.

Funding statement

This research was not at any stage funded by any commercial, governmental or not-for-profit organization.

Authors' contributions

Sanni Samuel conceived the idea of developing the manuscript, presented the paper-frame work, designed the work flow, as well as drafted and edited the final version of the manuscript. Oluranti Agboola and Peter Alaba made substantial contributions in terms of discussing the reaction mechanisms. Emeka Okoro and Moses Emetere contributed few sections of the write-up in line with other methods of producing hydrogen fuel. Babalola Oni and Amanda Ndubuisi helped with language editing, and establishing the chemistry and mechanisms of few reactions defined in the manuscript.

Declaration of Competing Interest

The authors declare that they have no known competing financial interests or personal relationships that could have appeared to influence the work reported in this paper.

Acknowledgement

The authors wish to appreciate Samuel Sanni for conceptualising the thought of putting together the manuscript. Oluranti Agboola, Peter Adeniyi Alaba and Emeka Okoro are all appreciated, for their meaningful discussions and contributions at different stages of the work.

References

[1] Spath PL, Mann MK. Life Cycle Assessment of Hydrogen Production via Natural Gas Steam Reforming, Technical Report, National Renewable Energy Laboratory, NREL/TP-570-27637. DOI: 10.2172/764485.
[2] Camacho YSM, et al. Development of a robust and efficient biogas processor for hydrogen production. Part 1: Modelling and simulation. Int J Hydro Energy 2017; 42:22841–55.
[3] Bareiß K, De la Rua C, Möckl M, Hamacher T. Life cycle assessment of hydrogen from proton exchange membrane water electrolysis in future energy systems. Appl Energy 2019;237:862–72.
[4] Navlani-Garcia M, Mori K, Salinas-Torres D, Kuwahara, YYamashita H. New approaches toward the hydrogen production from formic acid dehydration over Pd-based heterogeneous catalysts. Front Mater 2019;6:44. https://doi.org/10.3389/fmats.201900044.
[5] Buffoni IN, Gatti MN, Santori GF, Pompeo F, Nichio NN. Hydrogen from glycerol steam reforming with a platinum catalyst supported on a SiO2-C composite. Int J Hydro Energy 2017;42:12967–77.
[6] Charisiou ND, Siakavelas G, Papageridis KN, Baklavaridis A, Tzounis L, Polychronopoulou K, et al. Hydrogen production via the glycerol steam reforming reaction over nickel supported on alumina and lanthana-alumina catalysts. Int J Hydro Energy 2017;42:13039–60.
[7] Wang Y-Z, Zhang L, Xu T, Ding K. Influence of initial anolyte pH and temperature on hydrogen production through simultaneous saccharification and fermentation of lignocellulose in microbial electrolysis cell. Int J Hydro Energy 2017;42: 22663–70.
[8] Wang Y, Chen KS, Mishler J, Cho SC, Adroher XC. A review of polymer electrolyte membrane fuel cells: technology, applications, and needs on fundamental research. Appl Energy 2011;88:981–1007.
[9] Ahmed S, Krumpelt M. Hydrogen from hydrocarbon fuels for fuel cells. Int J Hydro Energy 2001;26:291–301.
[10] Jakobsen RJ, Mikawa Y, Brasch JW. Far infrared studies of hydrogen bonding in carboxylic acids-I formic and acetic acids. Spectrochim Acta A Mol Biomol Spectrosc 1967;23(7):2199–209.
[11] Loges B, Boddien A, Gartner F, Junge H, Beller M. Catalytic generation of hydrogen from formic acid and its derivatives: useful hydrogen storage materials. Top Catal 2010;53:902–14.
[12] Bulushev DA, Beloshapkin S, Ross JRH. Hydrogen from formic acid decomposition over Pd and Au catalysts. Catal Today 2010;154:7–12.
[13] Hu C, Pulleri JK, Ting SW, Chan KY. Activity of Pd/C for hydrogen generation in aqueous formic acid solution. Int J Hydr Energy 2014;39:381–90.
[14] Sachtler WMH, Fahrenfort J. The catalytic decomposition of formic acid vapor on metals. Proc. Second. Intern. Congr. Catalysis. Technip. Paris 1961; p. 831.
[15] Boudart M, Djega-Mariadassou G. Kinetics of heterogeneous catalytic reactions. Princeton: Princeton University Press; 1984.
[16] Madix RJ. Reaction kinetics and mechanism on metal single crystal surfaces. In: Eley DD, Pines H, Weisz PB, editors. Advances in catalysis, 29. Academic Press; 1980. p. 1.
[17] Yoo JS, Abild-Pedersen F, Norskov JK, Studt F. Theoretical analysis of transition metal catalysts for formic acid decomposition. ACS Catal 2014;4:1226–33. https://doi.org/10.1021/cs400664z.
[18] Herron JA, Scaranto J, Ferrin P, Li S, Mavrikakas M. Trends in formic acid decomposition on model transition metal surfaces: a density functional theory study. ACS Catal 2014;4(12):4434–45. https://doi.org/10.1021/cs500737p.
[19] Zahmakiran M, Ozkar S. Metal nanoparticles in liquid phase catalysis; from recent advances to future goals. Nanoscale 2011;3(9):3462–81. https://doi.org/10.1155/2014/324089.
[20] Luque R, Varma RS, editors. Sustainale preparation of metal nanoparticles: methods and applications. London UK: RSC Publishing; 2012.
[21] White RJ, Luque R, Budarin VL, Clark JH, Macquarrie DJ. Supported metal nanoparticles on porous materials. Methods and applications. Chem Soc Rev 2009;38:481–94. https://doi.org/10.1039/B802654H.
[22] Campelo JM, Luna D, Luque R, Marinas JM, Romero AA. Sustainable preparation of supported metal nanoparticles and their applications in catalysis. Chem Sus Chem 2009;2(1):18–45. https://doi.org/10.1002/cssc.200800227.
[23] Astruc D, Lu F, Aranzaes JR. Nanoparticles as recyclable catalysts: the frontier between homogeneous and heterogeneous catalysis. Angew Chem Int Ed England 2005;44(48):7852–72. https://doi.org/10.1002/anie.200500766.
[24] Sanni SE, Alade TA, Agboola O, Alaba PA. Catalytic dehydrogenation of formic acid triethanolamine mixture using copper nanoparticles. Int J Hydro Energy 2020;45(7):4606–24. https://doi.org/10.1016/j.ijhydene.2019.12.121.
[25] Crampton L. Formic acid dangers and uses in nature and humans. Owlcation, a Maven Channel, 2020.
[26] Fierro JLG. Hydrogen: production methods. Instituto de Catálisis y Petroleoquímica (CSIC); 2019. www.fgcsic.es/lychnos/en_en/articles/hydrogen_production_methods. Accessed December, 2019.
[27] Johnson TC, Morris DJ, Wills M. Hydrogen generation from formic acid and alcohols using homogeneous catalysts. Chem Soc Rev 2010; 39: 81-8.
[28] Do JY, Kwak BS, Kuk-Park N, Lee TJ, Lee ST, Jo SW, et al. Effect of Acidity on the performance of a Ni-based catalyst for hydrogen production through propane steam reforming: K-AlSi$_x$O$_y$ support with different Si/Al ratios. Int J Hydro Energy 2017;42:22687–97.
[29] Bareiß K, del Rua C, Möckl M, Hamacher T. Life cycle assessment of hydrogen from proton exchange membrane water electrolysis in future energy systems. Appl Energy 2019;237:862–72.
[30] Chin HL, Chen ZS, Chou CP. Fed batch operation using Clostridium acetobutylicum suspension culture as biocatalyst for enhancing hydrogen production. Biotechnol Prog 2003;19:383–8.
[31] Kumar N, Das D. Continuous hydrogen production by immobilized *Enterobacter Cloacae* IIT-BT 08 using lignocellulosic materials as solid matrices. Enzyme Microb Technol 2001;29:280–7.
[32] Melis A, Happe T. Hydrogen production. Green algae as a source of energy. Plant Physiol 2001;127:740–8.
[33] Nandi R, Bhattacharya PK, Bhaduri AN, Sengupta S. Synthesis and lysis of formate by immobilized cells of Escherichia coli. Biotechnol Bioeng 1992;39:775–80.
[34] Tsygankov AA, Hirata Y, Miyake M, Asada Y, Miyake J. Photobioreactor with photosynthetic bacteria immobilized on porous glass for hydrogen photo production. J Ferment Bioeng 1994;77:575–8.
[35] Lee KS, Lo YS, Lo YC, Lin PJ, Chang JS. H_2 production with anaerobic sludge using activated-carbon supported packed-bed bioreactors. Biotechnol Lett 2003; 25:133–8.
[36] Woodward J, Orr M, Cordray K, Greenbaum E. Enzymatic production of biohydrogen. Nature 2000;405:1014–5.
[37] Alexeeva S, Hellingwerf KJ, De Mattos MJT. Requirement of ArcA for redox regulation in Escherichia coli under microaerobic but not anaerobic or aerobic conditions. J Bacteriol 2003;185:204–9.
[38] Yoshida A, Nishimura T, Kawaguchi H, Inui M, Yukawa H. Enhanced hydrogen production from formic acid by formate hydrogen Lyase-overexpressing *Escherichia coli* strains. Appl Environ Microbiol 2005:6762–8. https://doi.org/10.1128/AEM.71.11.6762-6768.2005.
[39] De-Vos P, Stevens P, De-Lay J. Hydrogen gas production from formate and glucose by different members of *enterobactericeae*. Biotechnol Lett 1983;5:69–74.
[40] Kawamura S, O'Neil JG, Wilkinson JF. Hydrogen production by methylotrophs under anaerobic conditions. J Ferment Technol 1983;61:151–6.
[41] Schon G, Voelskow H. Pyruvate fermentation in Rhodospirillum rubrum and after transfer from aerobic to anaerobic conditions in the dark. Arch Microbiol 1976; 107:87–92.
[42] Alotaibi MH, Alotaibi RL, Aldosari OF. Hydrogen generation from formic acid decomposition using an Iradium-Palladium (Ir-Pd) nanoparticles supported on different supports. 24th Global Organic & Inorganic Chemistry Conference, Organic Chem. Curr. Res. 2018; 7: 43. DOI: 10.4172/2161-0401-C3-028.
[43] Sigma-Adrich. (2011). Sigma-aldrich. Accessed August 8, 2019. www.sigmaaldrich.com/MSD/.
[44] Aguilo A, Horlenko T. Formic acid. MacKetta JJ, Cunningham WA (Eds.), In: Encyclopedia of chemical processing and design, Marcel Dekker, Inc., New York, 1988; 23: 371-397.
[45] Reutemann W, Kieczka H. Formic acid, In Elvers B, Hawkins S, Ravenscroft M, Rounsaville JF, Schulz G (Eds.), Ullmann's encyclopedia of industrial chemistry, 5th ed., A12: 13-33 Wiley-VCH, Weinheim, Germany, 1996.
[46] Bulushev DA, Beloshapkin S, Ross JRH. Hydrogen from formic acid decomposition over Pt and Au Catalysts. Catal Today 2010;154:7–12. https://doi.org/10.1016/j.cattod.2010.03.050.
[47] Xue-li L, Feng S, Xiang-yuan M, Liu-jin L, You-Quan D. (2010). Selective catalytic formic acid decomposition for hydrogen generation in ionic liquids. J. Fuel Chem. Technol., 2010; 38, 5: 544-553.
[48] Sanchez F, Motta D, Roldan A, Hammond C, Villa A, Dimitratos N. Hydrogen generation from additive-free formic acid decomposition under mild conditions

by Pd/C: experimental and DFT studies. Top. Catal. Article in Press. https://doi.org/10.1007/s11244-018-0894-5.
[49] Müller K, Brooks K, Autrey T. Hydrogen storage in formic acid: a comparison of process options. Energy Fuels 2017;31:12603–11. https://doi.org/10.1021/acs.energyfuels.7b02997.
[50] Li S, Scaranto J, Mavrikakis M. On the structure sensitivity of formic acid decomposition on Cu catalysts. Top Catal 2016;2016(59):1580–8. https://doi.org/10.1007/s11244-016-0672-1.
[51] Columbia MR, Thiel PA. The interaction of formic-acid with transition metal surfaces, studied in ultrahigh vacuum. J Electroanal Chem 1994;369(1–2):1–14.
[52] Madix RJ. Surface reaction modifiers—general overview. Abstracts of papers of the American Chemical Society, 1980; 180: 26.
[53] Larson LA, Dickinson JT. Decomposition of formic acid on Ru(1010). Surf Sci 1979;84(1):17–30.
[54] Solymosi F, Kiss J, Kovacs I. Adsorption of HCOOH on Rh(111) and its reaction with preadsorbed oxygen. Surf Sci 1987;192(1):47–65.
[55] Senanayake SD, Mullins DR. Redox pathways for HCOOH decomposition over CeO2 surfaces. J Phys Chem C 2008;112(26):9744–52.
[56] Kubota J, Bandara A, Wada A, Domen K, Hirose C. IRAS study of formic acid decomposition on NiO(111)/Ni(111) surface: comparison of vacuum and catalytic conditions. Surf Sci 1996;368:361–5.
[57] Dilara PA, Vohs JM. TPD and HREELS investigation of the reaction of formic acid on ZrO_2(100). J Phys Chem 1993;97(49):12919–23.
[58] Iglesia E, Boudart M. Decomposition of formic acid on copper, nickel, and copper–nickel alloys. Catalytic and temperature-programmed decomposition of formic acid on Cu/SiO_2, Cu/Al_2O_3, and Cu powder. J Catal 1983;81(1):214–23.
[59] Bowker M, Madix RJ. XPS, UPS and thermal desorption studies of the reactions of formaldehyde and formic acid with the Cu(110) surface. Surf Sci 1981;102(2–3):542–65.
[60] Marcinkowski MD, Murphy CJ, Liriano ML, Wasio NA, Lucci FR, Sykes ECH. Microscopic view of the active sites for selective dehydrogenation of formic acid on Cu(111). ACS Catal 2015;5(12):7371–8.
[61] Youngs TGA, Haq S, Bowker M. Formic acid adsorption and oxidation on Cu (110). Surf Sci 2008;602(10):1775–82.
[62] Bowker M, Haq S, Holroyd R, Parlett PM, Poulston S, Richardson N. Spectroscopic and kinetic studies of formic acid adsorption on Cu(110). J Chem Soc Faraday Trans 1996;92(23):4683–6.
[63] Quinn DF, Taylor D. Decomposition of formic acid and methanol on copper–nickel alloys. J Chem Soc 1965:5248–51.
[64] Rundell DN, Saltsburg HM, Smith WD. The role of multiple gas-solid collisions in the catalytic decomposition of formic acid. Chem Eng Sci 1980;35(5):1113–9.
[65] Inglis HS, Taylor D. Decomposition of formic acid on titanium, vanadium, chromium, manganese, iron, cobalt, nickel and copper. J Chem Soc Inorg Phys Theor 1969;19:2985–7.
[66] Nakano H, Nakamura I, Fujitani T, Nakamura J. Structuredependent kinetics for synthesis and decomposition of formate species over Cu(111) and Cu(110) model catalysts. J Phys Chem B 2001;105(7):1355–65.
[67] Hu ZM, Boyd RJ. Structure sensitivity and cluster size convergence for formate adsorption on copper surfaces: a DFT cluster model study. J Chem Phys 2000;112(21):9562–8.
[68] Bowker M, Rowbotham E, Leibsle FM, Haq S. The adsorption and decomposition of formic acid on Cu{110}. Surf Sci 1996;349(2):97–110.
[69] Gokhale AA, Dumesic JA, Mavrikakis M. On the mechanism of low-temperature water gas shift reaction on copper. J Am Chem Soc 2008;130(4):1402–14.
[70] Grabow LC, Gokhale AA, Evans ST, Dumesic JA, Mavrikakis M. Mechanism of the water gas shift reaction on Pt: first principles, experiments, and microkinetic modeling. J Phys Chem C 2008;112(12):4608–17.
[71] Caner N, Buluta A, Yurderia M, Ertasa IE, Kivrakb H, Kayac M, et al. Atomic layer deposition-SiO_2 layers protected PdCoNi nanoparticles supported on TiO_2 nanopowders: exceptionally stable nano catalyst for the dehydrogenation of formic acid. Appl Catal B: Environ 2017;210:470–83.
[72] Wachs IE. Raman and IR studies of surface metal oxide species on oxide supports: Supported metal oxide catalysts. Catal. Today 1996; 27: 437-455. SSDI 0920-5861(95)00203-0.
[73] Sadovskaya EM, Chesalov YA, Goncharova VB, Soboleva VI, Andrushkevicha TV. Formic acid decomposition over V-Ti oxide catalyst: mechanism and kinetics. J Molecular Catal A: Chem 2017;430:54–62.
[74] Liu D, Gao ZY, Wang XC, Zeng J, Li YM. DFT study of hydrogen production from formic acid decomposition on Pd-Au alloy nanoclusters. Appl Surf Sci 2017;426:194–205. https://doi.org/10.1016/j.apsusc.2017.07.165.
[75] Zavras A, Khairallah GN, Krstić M, Girod M, Daly S, Antoine R, et al. Ligand-induced substrate steering and reshaping of $[Ag_2(H)]^+$ scaffold for selective CO_2 extrusion from formic acid. Nat Commun 2016;7:11746. https://doi.org/10.1038/ncomms11746.
[76] Edwards JK, Ntainjua E, Carley AF, Herzing AA, Kiely CJ, Hutchings GJ. Direct synthesis of H_2O_2 from H_2 and O_2 over gold, palladium, and gold-palladium catalysts supported on acid-pretreated TiO_2. Angew Chem Int Ed 2009;48:8512–5.
[77] Edwards JK, Solsona B, Ntainjua E, Carley AF, Herzing AA, Kiely GJ, et al. Switching off hydrogen peroxide hydrogenation in the direct synthesis process. Science 2009;323:1037–41.
[78] Allison EG, Bond GC. The structure and catalytic properties of palladium-silver and palladium-gold alloys. Catal Rev 1972;7:233–89.
[79] Zhu Q-L, Tsumori N, Xu Q. Sodium hydroxide-assisted growth of uniform Pd nanoparticles on nanoporous carbon MSC-30 for efficient and complete dehydrogenation of formic acid under ambient conditions. Chem Sci 2014;5:195–9.
[80] Zhou X, Huang Y, Xing W, Liu C, Liao J, Lu T. High-quality hydrogen from the catalysed decomposition of formic acid by Pd-Au/C and Pd-Ag/C. Chem Commun 2008:3540–2.
[81] Bi QY, Du XL, Liu YM, Cao Y, He HY, Fan KN, Efficient subnanometric gold-catalyzed hydrogen generation via formic acid decomposition under ambient conditions J. Am. Chem. Soc. 2012; 134, 21: 8926-8933. Doi: 10.1021/ja301696e.
[82] Tedsree K, Li T, Jones S, Chan CWA, Yu KMK, Bagot PAJ, et al. Hydrogen production from formic acid decomposition at room temperature using an Ag-Pd core-shell nanocatalyst. Nat Nanotechnol 2011;6:302–7.
[83] Wang Z-L, Yan J-M, Wang H-L, Ping Y, Jiang Q. Au@Pd core-shell nanoclusters growing on nitrogen-doped mildly reduced graphene oxide with enhanced catalytic performance for hydrogen generation from formic acid. J Mater Chem 2013;A1:12721–5.
[84] Wang ZL, Yan JM, Ping Y, Wang HL, Zheng WT, Jiang Q. An efficient CoAuPd/C catalyst for hydrogen generation from formic acid at room temperature. Angew Chem Int Ed 2013;2(16):4406–9. https://doi.org/10.1002/anie.201301009.
[85] Wang ZL, Wang HL, Yan JM, Ping Y, Li SJ, Jiang Q. DNA-directed growth of ultrafine CoAuPd nanoparticles on graphene as efficient catalysts for formic acid dehydrogenation. Chem Commun 2014;50(21):2732–4. https://doi.org/10.1039/c3cc49821b.
[86] Metin Ö, Sun X, Sun S. Monodisperse gold–palladium alloy nanoparticles and their composition-controlled catalysis in formic acid dehydrogenation under mild conditions. Nanoscale 2013;5:910–2.
[87] Karatas Y, Bulut A, Yurderi M, Ertas IE, Alal O, Gulcan M, et al. PdAu-MnOxnanoparticles supported on amine-functionalized SiO_2 for the room temperature dehydrogenation of formic acid in the absence of additives. Appl Catal B: Environ 2016;180:586–95. https://doi.org/10.1016/j.apcatb.2015.06.060.
[88] Bulut A, Yurderi M, Karatas Y, Say Z, Kivrak H, Kaya M, et al. MnOx-promoted PdAg alloy nanoparticles for the additive-free dehydrogenation of formic acid at room temperature. ACS Catal 2015;5:6099–110. https://doi.org/10.1021/acscatal.5b01121.
[89] Yurderi M, Bulut A, Caner N, Elebi MC, Kaya M, Zahmakiran M. Amine grafted silica supported CrAuPd alloy nanoparticles: superb heterogeneous catalysts for the room temperature dehydrogenation of formic acid. Chem Commun 2015;57:11417–20. https://doi.org/10.1039/C5CC02371H.
[90] Yurderi M, Bulut A, Zahmakiran M, Kaya M. Carbon supported trimetallic PdNiAg nanoparticles as highly active, selective and reusable catalyst in the formic acid decomposition. Appl Catal B: Environ 2014;160–161:514–24. https://doi.org/10.1016/j.apcatb.2014.06.004.
[91] Bulut A, Yurderi M, Karatas Y, Zahmakiran M, Kivrak H, Gulcan M, et al. Pd-MnOx nanoparticles disperse donamine grafted silica: highly efficient nanocatalyst for hydrogen production from additive-free dehydrogenation of formic acid under mild conditions. Appl Catal B Environ 2015;164:324–33. https://doi.org/10.1016/j.apcatb.2014.09.041.
[92] Yan J-M, Wang Z-L, Gu L, Li S-J, Wang H-L, Zheng W-T, Jiang Q. AuPd–MnOx/MOF–graphene: an efficient catalyst for hydrogen production from formic acid at room temperature. Adv Energy Mater 2015; pp. 15001001–1500107. DOI: 10.1002/aenm.201500107.
[93] Wang ZL, Yan JM, Wang HL, Ping Y, Jiang Q. Au@Pd core–shellnanoclusters growing on nitrogen-doped mildly reduced graphene oxidewith enhanced catalytic performance for hydrogen generation from formic acid. J Mater Chem A 2013;1:12721–5.
[94] Zhou X, Huang Y, Xing W, Liu C, Liao J, Lu T. High-quality hydrogen from the catalyzed decomposition of formic acid by Pd-Au/C and Pd-Ag/C. Chem Commun 2008;30:3540–2.
[95] Huang Y, Zhou X, Yin M, Liu C, Xing W. Novel PdAu@Au/C core-shellcatalyst: superior activity and selectivity in formic acid decomposition for hydrogen generation. Chem Mater 2010;22:5122–8.
[96] Gu X, Lu ZH, Jiang HL, Akita T, Xu Q. Synergistic catalysis of metal–organic framework-immobilized Au–Pd nanoparticles in dehydrogenation of formic acid for chemical hydrogen storage. J Am Chem Soc 2011;133:11822–5.
[97] Wang ZL, Yan JM, Ping Y, Wang HL, Zheng WT, Jiang Q. An efficient CoAuPd/C catalyst for hydrogen generation from formic acid at room temperature. Angew Chem Int Ed 2013;52:4406–9.
[98] Yu WY, Mullen GM, Flaherty DW, Mullins CB. Selective hydrogen production from formic acid decomposition on Pd-Au bimetallic surfaces. J Am Chem Soc 2014;136:11070–8.
[99] Yan JM, Wang ZL, Gu L, Li SJ, Wang HL, Zheng WT, et al. An efficient catalyst for hydrogen production from formic acid at room temperature. Adv Energy Mater 2015;5:1500107.
[100] Detwiler MD, Milligan CA, Zemlyanov DY, Delgass WN, Ribeiro FH. Kinetics of gas phase formic acid decomposition on platinum single crystal and polycrystalline surfaces. Surf Sci 2016;648:220–6.
[101] Navlani-García M, Mori K, Kuwahara Y, Yamashita H. Recent strategies targeting efficient hydrogen production from chemical hydrogen storage materials over carbon-supported catalysts. NPG Asia Mater 2018;10:277–92. https://doi.org/10.1038/s41427-018-0025-6.
[102] Wang Y, Qi Y, Zhang D, Liu C. New insight into the decomposition mechanism of formic acid on Pd(111): competing formation of CO_2 and CO. J Phys Chem C 2014;118:2067–76.

[103] Tang Y, Roberts CA, Perkins RT, Wachs IE. Revisiting formic acid decomposition on metallic powder catalysts: exploding the HCOOH decomposition volcano curve. Surf Sci 2016;650:103–10.

[104] Ojeda M, Iglesia E. Formic acid dehydrogenation on au-based catalysts at near-ambient temperatures. Angew Chem Int Ed 2009;48(26):4800–3. https://doi.org/10.1002/anie.200805723.

[105] Jia L, Bulushev D, Ross JRH. Formic acid decomposition over palladium catalysts doped by potassium carbonate. Catal Today 2016;259:453–9.

[106] Silbaugh TL, Karp EM, Campbell CT. Energetics of methanol and formic acid oxidation on Pt (111): mechanistic insights from adsorption calorimetry. Surf Sci 2016;650:140–3.

[107] Suenobu T, Shibata S, Fukuzumi S. Catalytic oxidation of formic acid by dioxygen with an organoiridium complex. Catal Sci Technol 2014;4:3636–9. https://doi.org/10.1039/C4CY00957F.

[108] Celaje JJA, Lu Z, Kedzie EA, Terrile NJ, Lo JN, Williams TJ. A prolific catalyst for dehydrogenation of neat formic acid. Nat Commun 2016;7:11308–13. https://doi.org/10.1038/ncomms11308.

[109] Noto Y, Fukuda K, Onishi T, Tamaru K. Mechanism of formic acid decomposition over dehydrogenation catalysts. Trans Faraday Soc 1967;63:3081–7.

[110] Zhong H, Iguchi M, Song F-Z, Chatterjee M, Ishizaka T, Nagao I, et al. Automatic high-pressure hydrogen generation from formic acid in the presence of nano-Pd heterogeneous catalysts at mild temperatures. Sust Energy Fuels 2017;1:1049–55.

[111] Li Z, Xu Q. Metal-nanoparticle-catalyzed hydrogen generation from formic acid. Acc Chem Res 2017;50(6):1449–58. https://doi.org/10.1021/acs.accounts.7b00132.

[112] Jiang Q, Lu HM, Zhao M. Modelling of surface energies of elemental crystals. J Phys Condens Matter 2004;16:521–30.

[113] Yi CW, Luo K, Wei T, Goodman DW. The composition and structure of Pd-Au surfaces. J Phys Chem B 2005;109:18535–40.

[114] Ding Y, Fan F, Tian Z, Wang ZL. Atomic structure of Au-Pd bimetallic alloyed nanoparticles. J Am Chem Soc 2010;132:12480–6.

[115] Dong W, Hafner J. H_2 dissociative adsorption on Pd (111). Phys Rev B 1997;56:15396–403.

[116] Singh S, Li S, Carrasquillo-Flores R, Alba-Rubio AC, Dumesic JA, Mavrikakis M. Formic acid decomposition on Au catalysts: DFT, microkinetic modeling, and reaction kinetics experiments. AIChE J 2014;60:1303–19.

[117] Yu WY, Mullen GM, Mullins CB. Hydrogen adsorption and absorption with Pd-Au bimetallic surfaces. J Phys Chem C 2013;117:19535–43.

[118] Yadav M, Xu Q. Liquid-phase chemical hydrogen storage materials. Energy Environ Sci 2012;5:9698–725. https://doi.org/10.1039/C2EE22937D.

[119] Mackay GI, Hopkinson AC, Bohme DK. Acid catalysis in the gas phase: dissociative proton transfer to formic and acetic acid. J Am Chem Soc 1978;100(24):7460–4. https://doi.org/10.1021/ja00492a003.

[120] Holmes JL, Mommers AA, De Koster C, Heerma W, Terlouw JK. Four isomeric $[C, H_3, O_2]^+$ ions. Chem Phys Lett 1985;115:437–40.

[121] Sekiguchi O, Bakken V, Uggerud E. Decomposition of protonated formic acid: one transition state-two product channels. J Am Soc Mass Spectrom 2004;15:982–8.

[122] Lias SG, Rosenstock HM, Deard K, Steiner BW, Herron JT, Holmes JH et al. NIST Chemistry Web book, 2002. (http://webbook.nist.goc/ chemistry).

[123] Wang Z, Hao X, Hu D, Li L, Song X, Zhang W, et al. PdAu bimetallic nanoparticles anchored on amine-modified mesoporous ZrSBA15 for dehydrogenation of formic acid at ambient conditions. Electronic Supplementary Material (ESI). Catal Sci Technol 2017.

[124] Bi QY, Lin JD, Liu YM, He HY, Huang FQ, Cao Y. Dehydrogenation of formic acid at room temperature: boosting palladium nanoparticle efficiency by coupling with pyridinic nitrogen-doped carbon. Angew Chem Int 2016;55:11849–53. https://doi.org/10.1002/anie.201605961.

[125] Zhang S, Metin Ö, Su D, Sun S. Monodisperse AgPd alloy nanoparticles and their superior catalysis for the dehydrogenation of formic acid. Angew Chem Int Ed 2013;52:3681–4.

[126] Wang ZL, Ping Y, Yan JM, Wang HL, Jiang Q. Hydrogen generation from formic acid decomposition at room temperature using a NiAuPd alloy nanocatalyst. Int J Hydr Energy 2014;39:4850–6.

[127] Li SJ, Ping Y, Yan JM, Wang HL, Wu M, Jiang Q. Facile synthesis of AgAuPd/graphene with high performance for hydrogen generation from formic acid. J Mater Chem A 2015;3:14535–8. https://doi.org/10.1039/C5TA03111G.

[128] Wang ZL, Wang HL, Yan Ping, Li YsioSJ, Jiang Q. DNA-directed growth of ultrafine CoAuPd nanoparticles on graphene as efficient catalysts for formic acid dehydrogenation. Chem Commun 2014;50:2732–4. https://doi.org/10.1039/c3cc49821b.

[129] Wang ZL, Yan JM, Zhang YF, Ping Y, Wang HL, Jiang Q. Facile synthesis of nitrogen-doped graphene supported AuPd–CeO_2 nanocomposites with high-performance for hydrogen generation from formic acid at room temperature. Nanoscale 2014;6:3073–7.

[130] Ke F, Wang L, Zhu J. An efficient room temperature core–shell AgPd@MOF catalyst for hydrogen production from formic acid. Nanoscale 2015;7(18):8321–5. https://doi.org/10.1039/C4NR07582J.

[131] Koh K, Seo JE, Lee JH, Goswami A, Yoon CW, Asefa T. Ultrasmall palladium nanoparticles supported on amine-functionalized SBA-15 efficiently catalyze hydrogen evolution from formic acid. J Mater Chem A 2014;2:20444–9. https://doi.org/10.1039/C4TA04538F.

[132] Sun Q, Wang N, Bing RS, Liu J, Bai R, Zhang P, et al. Subnanometric Hybrid Pd-M(OH)2, M = Ni Co, Clusters in Zeolites as Highly Efficient Nanocatalysts for Hydrogen Generation. Chem 2017;3:477–93. https://doi.org/10.1016/j.chempr.2017.07.001.

[133] Benck JD, Hellstern TR, Kibsgaard J, Chakthranont P, Jaramillo TF. Catalyzing the Hydrogen Evolution Reaction (HER) with Molybdenum Sulfide Nanomaterials. ACS Catal. 2014; 4: 3957-3971. dx.doi.org/10.1021/cs500923c.

[134] Scotti N, Psaro R, Ravasio N, Zaccheria F. A new Cu-based system for formic acid dehydrogenation. RSC Adv 2014.

[135] Zhu Q-L, Tsumori N, Xu Q. Immobilizing extremely catalytically active palladium nanoparticles to carbon nanospheres: a weakly-capping growth approach. J Am Chem Soc 2015;137:11743–8.

[136] Bielinski EA, Lagaditis PO, Zhang Y, Mercado BQ, Würtele C, Bernskoetter WH, et al. Lewis acid-assisted formic acid dehydrogenation using a pincer-supported iron catalyst. J Am Chem Soc 2014;136:10234–7.

[137] Sanni SE, Ewetade AP, Emetere ME, Agboola O, Okoro E, Olorunshola SJ, et al. Enhancing the inhibition potential of sodium tungstate towards mitigating the corrosive effect of Acidithiobaccillus thiooxidan on X-52 carbon steel. Mater Today Commun 2019;19:238–51. https://doi.org/10.1016/j.mtcomm.2018.12.010.

[138] James B, Bushman P. Corrosion and cathodic protection theory. Int J Renew Energy Res 2014;4:3–10.

[139] Mannari V, Patel CJ. Introduction to paints and coatings. In: understanding raw materials, introduction to paints and coatings, Vincentz Network, Hanover, Germany, Ch. 1, pp. 19-27, 2015. ISBN: 978-3-86630-603-5.

[140] Sanni SE, Adefila SS, Anozie AN. Prediction of sand kinematic pressure and fluid particle interaction coefficient as means of preventing sand-induced corrosion in crude oil pipelines. Ain Shams Eng'g J 2019;10:55–62.

[141] Sugama T. High-Performance Coating Materials. Energy sciences and technology department/energy resources division, Brookhaven National Laboratory, 2006. BNL-77900-2007-IR.

[142] Kelly PJ, Hisek J, Zhou Y, Pilkington RD, Arnell RD. Advanced coatings through pulsed magnetron sputtering. Surf Eng'g 2004;20(3):157–62. https://doi.org/10.1179/026708404225010702.

[143] Ngobiri NC, Oguzie EE, Oforka NC, Akaranta O. Comparative study on the inhibitive effect of Sulfadoxine–Pyrimethamine and an industrial inhibitor on the corrosion of pipeline steel in petroleum pipeline water, Arab. J. Chem., 2015; 1–11, Article in Press.

[144] Li E, Wu J, Zhang D, Sun Y, Chen J. D-phenylalanine inhibits the corrosion of Q235 carbon steel caused by *Desulfovibrio Sp*. Int Biodeter Biodegrad 2018;127:178–84. https://doi.org/10.1016/j.ibiod.2017.11.027.

[145] Héctor AV, Liz KH. Microbiologically influenced corrosion: looking to the future. Int Microbiol 2005;8:169–80.

[146] Sanni SE, Fayomi SIO, Emetere ME, Tenebe TI. Corrosion inhibition of mild steel in aqueous HCL using bitter leaf and fenugreek seed oils. Pro Metals Phys Chem Surf 2019;55(2):389–99. https://doi.org/10.1134/S2070205119020254.

[147] Agboola O, Achile F, Fayomi SO, Sanni SE, Abatan O, Sadiku ER, et al. Adsorptive performance mechanism of the DNA of calf thymus gland (CTGDNA) on 3CR12 stainless steel as corrosion inhibitor in acidic medium. J Bio-Tribo-Corr 2019;5(52):1–17. https://doi.org/10.1007/s40735-019-0245-5.

[148] Okafor PC, Ikpi ME, Uwah IE, Ebenso EE, Ekpe UJ, Umoren UJ. Inhibitory action of Phyllanthus amarus extracts on the corrosion of mild steel in acidic media. Corros Sci 2008;50:2317. https://doi.org/10.1016/jcorsci.2008.05.009.

[149] Ostovari A, Hoseinieh SM, Peikari M, Shadizadeh SR, Hashemi SJ. Corrosion inhibition of mild steel in 1 M HCl solution by henna extract: a comparative study of the inhibition by henna and its constituents (Lawsone, gallic acid, a-D-glucose and tannic acid). Corros Sci 1949;2009:50. https://doi.org/10.1016/jcorsci.2008.05.024.

[150] Balasubramanyam N, Prasanthi SG, Yugandhar M. Study of coated TiN and TiC on cutting tools for the PVD and CVD coated tungsten carbide by sand blasting pretreatment of nickel and carbon. Int J Adv Sci Technol 2015;75:51–8. https://doi.org/10.14257/ijast.2015.75.06.

[151] Sander G, Tan J, Balan P, Gharbi O, Feenstra DR, Singer L, et al. Corrosion of additively manufactured alloys: a review. Corrosion 2018;74(12):1318–50.

[152] Tedsree K, Li T, Jones S, Chan CWA, Yu KMK, Bagot PAJ, et al. Hydrogen production from formic acid decomposition at room temperature using a Ag-Pd core-shell nanocatalyst. Nat Nanotechnol 2011;6:302–7.

[153] Wang ZL, Wang HL, Yan JM, Ping SIO, Li SJ, Jiang Q. DNA-directed growth of ultrafine CoAuPd nanoparticles on graphene as efficient catalysts for formic acid dehydrogenation. Chem Commun 2014;50:2732–4. https://doi.org/10.1039/c3cc49821b.

[154] Akbayraka S, Tonbul Y, Özkar S. Nanoceria supported palladium(0) nanoparticles: Superb catalyst in dehydrogenation of formic acid at room temperature. Appl Catal B: Environ 2017;206:384–92.

[155] https://www.ballonbau.de/en/sport-balloons.